UNIVERSITY OF MICHIGAN

DEPARTMENT OF MECHANICAL ENGINEERING

ANN ARBOR, MI 48109

TECHNICAL REPORT UM-MEAM-96-18

DECOMPOSITION ANALYSIS OF AN AUTOMOTIVE POWERTRAIN DESIGN PROBLEM: MODEL DEVELOPMENT, PARTITIONING, AND OPTIMIZATION

TERRANCE C. WAGNER * and PANOS Y. PAPALAMBROS **

**Ford Motor Company, Powertrain Division, Dearborn, Michigan , USA*

***Automotive Research Center, The University of Michigan, Ann Arbor, Michigan 48109, USA*

(Submitted August 1996)

Using the nonlinear programming paradigm, *decomposition analysis* is a rigorous method for reformulating a system design problem into a coordination problem of simultaneous design optimization of subsystems. Decomposition methods in mathematical programming typically apply a coordination strategy based on an identifiable structure in the problem. Decomposition analysis aims at discovering how to (i) partition an original model so that the resulting problem structure matches the one required by a general coordination strategy, and (ii) implement the most suitable such strategy. Automated partitioning has received significant attention recently but implementation of coordination strategies using decomposition analysis is still scarce. This article presents a complete decomposition analysis, i.e., optimization model development, partitioning, and coordinated solution, for an automotive powertrain design problem. The model is presented in some detail and offers a practical approach for accommodating control and geometry variables simultaneously. A variable complexity coordination strategy is proposed and implemented.

KEY WORDS: optimal design, decomposition, coordination methods, automotive powertrain

1 INTRODUCTION

The recent industrial emphasis on shorter product development cycles has increased the need for properly coordinated solution of engineering system design problems. Generally, decomposition allows a system design problem to be solved as a set of smaller subsystem design problems properly coordinated to meet system design goals. Specifically, in nonlinear programming (NLP), decomposition partitions the original NLP problem into a set of smaller NLP problems solved independently but coordinated by a master problem using an appropriate coordination strategy. Partitioning and coordination are distinct but interdependent phases of a decomposition method. If a design problem can be cast as an NLP problem and a decomposition method can be applied, the resulting overall solution strategy serves as an excellent paradigm for coordinated design.

Decomposition methods fall into three categories, feasible, dual, and dual-feasible. Each use linking variables to effect independent subproblems and a coordination strategy that solves for those variables in a master problem. In feasible methods linking variables are primal variables; in dual methods they are dual variables associated with respective linking constraints. Dual-feasible methods use both linking functions and variables to implement a decomposition. A specific decomposition method is designed around specific structure in the problem (Wismer 1971, Lasdon 1970, Cramer et al. 1993, Balling and Sobieszczanski-Sobieski 1994). However, the problem of rigorously identifying structure and relating it specifically to candidate coordination strategies has only recently been pursued.

Model-based decomposition (Wagner 1993) was developed to identify coordination strategies for both classical mathematical programming formulations and multi-disciplinary optimization (MDO) problems. A specific decomposition method is classified by defining properties which are translated into *partition metrics* that rigorously describe structure in the NLP problem. Using an undirected graph representation of the NLP problem, the partition metrics facilitate identification of desirable structure using a variety of partitioning techniques. This

representation facilitates decomposition of NLP problems and MDO optimization problems because of a subtle but important distinction - no precedence relationships among variables are specified a priori. In MDO problems, a directed graph is often used to partition the *sequence* of analysis tasks based on precedence relationships specified prior to partitioning (for example, Rogers 1989, Rogers and Bloebaum 1994, Altus et al. 1995). Directed graphs are not readily amenable to representing the NLP problem because the precedence relationships they require do not exist in an NLP problem until after the problem is solved. Only then are dependent and independent variables distinguished. Hence, we contend that model-based decomposition facilitates identification of broader set of coordination strategies for a given problem - those found in the NLP literature and those found in the MDO literature.

Model-based decomposition proceeds with the four phases shown in Figure 1: model development, partitioning, coordination strategy development, and, solution. If the objective function is identified prior to the partitioning process, we use *decomposition analysis* (Wagner op cit.) because an optimal design problem (ODP) is constructed and analyzed for decomposability. If the objective is selected after partitioning, such that a decomposable optimization problem is synthesized, we use *decomposition synthesis* (Krishnamachari 1996).

Model development consists of formulating the system model by defining variables, parameters, functional relationships, and constraints, and by translating desirable defining properties into partition *metrics* which define what linking properties are sought (variables vs. functions), the maximum and minimum number of linking properties, the minimum number of subproblems desired, the relative balance of subproblems, and any a priori preferences such as including a specific variable as a linking variable. Wagner (op cit.) classifies in detail defining properties for a broad class of NLP and MDO decomposition methods.

The partitioning process consists first of constructing the functional dependence table (FDT) of the NLP problem which is an incidence matrix of Booleans denoting whether a function is dependent on a variable. The undirected graph representation is then constructed and the optimal

partitions are sought using one of several approaches. Wagner and Papalambros (1993a, 1993b) used a k-clique formulation for the undirected graph and a heuristic search algorithm described shortly to identify the minimum number of linking variables resulting in an 'acceptable' number of disjoint partitions of a specified size. Michelana and Papalambros (1994, 1995) solved the optimal partitioning problem more rigorously, treating it first as a network reliability problem and then as a hypergraph problem that can be solved with global partitioning techniques (Hendrickson and Leland 1993). Krishnamachari and Papalambros (1996) used a bi-partite graph formulation which facilitates integer programming techniques to identify optimal partitions and allows even more explicit definition of the number and relative size of partitions.

Figure 2 shows the FDT for a simple optimization model (Hock and Schittkowski 1981) and the post-partitioned FDT using heuristic search. Several feasible decomposition methods having the generic strategy in Figure 3 could be used. For example, the decomposed solution (Wagner and Papalambros 1993b) using Wismer and Chattergy's strategy (1978) compares favorably to the original solution.

The article now presents a complete decomposition analysis of a powertrain design problem. The complete model is presented, the FDT is constructed and partitioned. The partitions result in a variable complexity coordination strategy that treats engine speed, engine torque, manifold pressure, and engine displacement as linking variables.

2 MODEL DEVELOPMENT

The vast literature in the Transactions of the Society of Automotive Engineers (SAE) reveals the depth to which vehicle and powertrain components are understood. However, synthesis of components into an optimal vehicle system has not been extensively studied. Powertrain optimization studies invariably invoke *aspect* decomposition, namely, some aspect of the powertrain is varied, for example, engine control strategy, valve timing, or transmission strategy, while the other design quantities are treated as fixed parameters. Furthermore, the effects

of changes in these parameters on the optimal design are rarely studied. The following is a limited review of literature where optimization has been used for powertrain component problems.

Reasonably complex models of combustion chambers (Davis et al. 1982, 1986, 1988; Newman et al. 1989), induction systems (Chapman et al. 1982), torque converters (Sakamoto et al. 1992), and other components have been developed to predict the effects of geometric design variables on component behavior. Optimal geometries have been attained both through parametric studies (Assanis and Polishak 1989) and through nonlinear programming (Lamancusa 1988, Woodard 1988, Tzannetakis 1994). Optimal control strategies have been sought for the engine (Auiler et al. 1977; Rishavy et al. 1977; Donner 1978), and the transmission (Niste 1989, Starkey 1988, Kuzak et al. 1984).

The focus of each of these studies has typically been one aspect of the powertrain, i.e., engine control strategy, transmission shift strategy, engine geometry, cam timing, etc., rather than examining several aspects simultaneously in the search for an optimal powertrain system design. The present study encompasses engine variables, control schedules of exhaust gas recirculation (egr), torque converter size, and gear ratios, to meet a combination of fuel economy, emissions, and performance objectives.

We now proceed with model development. We define the system boundary and constants, list all parameters and all design, state, and behavior variables, and develop relationships between functional criteria and variables. In some cases the relationships are represented by scalable experimental data. When constructing the FDT, such relationships are presented implicitly. Explicit values are needed for the actual optimization study. Those used here are given in Appendix B and discussed in the appropriate sections.

The system of interest, a four-wheeled passenger car on a road, has two boundaries: the atmosphere around the vehicle and the asphalt road at the wheels. The only system constants are the gravitational constant, g, and the road material, asphalt, since they are fixed for all analyses of

the vehicle. The atmospheric pressure, P_{air}, temperature, T_{air}, velocity, V_{air}, and the grade angle, α, are parameters that can take on different values for various functional criteria. For the analysis here the grade angle takes on various values.

Design variables describe either proportions or a control strategy. State variables can vary with time. Behavior variables are attributes at a specified state or a specified integral of states. Prior to partitioning no distinction is made between the type of variables; this is given some consideration only after the obtained partitions are examined. To maintain continuity in the presentation the variables are given in Appendix A and are described as they are introduced.

The principal design criteria of interest are: fuel economy, emissions, and accleration performance. Fuel economy and emissions directly affect profits. A vehicle that cannot be certified to meet emissions cannot be sold. In the U.S., manufacturer's fleet sales must satisfy a Corporate Average Fuel Economy (CAFE) standard or pay penalties proportional to the violation. The acceleration times are measures of a vehicle's perceived performance and market image. The distance a vehicle travels from rest in four seconds and the 5-20 mph acceleration time correlate with initial acceleration; the 0-60 mph acceleration time correlates with average vehicle acceleration over the speed range of the engine. Starting gradeability α_s is important for markets with hilly or mountainous terrain. Cruising velocity at grade V_c is the speed at which the vehicle can climb a six percent grade in fourth gear (applies to four and five speed vehicles). A six percent grade is the largest grade on most U.S. interstate highways. These criteria are by no means a comprehensive list. For example, 3-D vehicle stability analysis during cornering, braking, and crash avoidance is not considered, nor are noise, vibration, and harshness (NVH) criteria. However, the criteria shown and the variables required to analyze them are of sufficient breadth to represent critical tradeoffs — performance, emissions, and fuel economy— and constitute a sufficiently challenging optimization problem. Moreover, as the decomposition analysis will reveal, the problem is easily expandable.

The U.S. metro-highway fuel economy, expressed in units of miles per gallon, represents a weighted average of the fuel consumed over the city and highway driving cycles. In the U.S. Emissions Federal Test Procedure No. 75, oxides of nitrogen (NOx), carbon monoxide (CO), and hydrocarbons (HC) emissions are collected and 'bagged' over a three phase driving cycle. Standards set by the Clean Air Act (CAA) and the California Air Resources Board (CARB) dictate acceptable levels (i.e., set the constraint values). Bosch (1986) provides a good description of legislated driving cycles and test procedures worldwide. Only the emissions NO and NO_2, collectively referred to as NOx, are considered here. Hydrocarbons are ignored since approximately 80% of the total hydrocarbon emissions are emitted during the first 120 seconds of the cycle as the catalyst warms up to maximum efficiency; they are managed with control strategies for cold transient behavior which is beyond the scope of the problem formulated here. Similarly, catalyst efficiencies for CO are sufficient to the extent that CO emissions would rarely become an active design constraint.

Vehicle Relationships

Appendix A has the complete nomenclature used to describe the vehicle dynamics and Figure 4 shows a free body diagram for the vehicle. The driving equation for all the criteria is simply the balance of forces on the vehicle,

$$M\, dV/dt = F_d - F_{roll} - F_{grade} - F_{aero}. \qquad (1)$$

The vehicle acceleration is proportional to the driving force at the road-wheel interface and the resistive forces of rolling friction, gravity, and air drag. The rolling resistance is the sum of tire friction and brake drag on the wheels; tire friction is the product of the coefficient of rolling resistance and the normal force at the wheels; brake drag is measured or modeled and for decomposition analysis is given as function of wheel speed,

$$F_{roll} = C_{roll}\, F_{nnd} + C_{roll}\, F_{nd} + (T_{bd}\ (N_d) + T_{bnd}\, (V/r_e))/r_e \qquad (2)$$

The rolling coefficient, C_{roll}, is often determined experimentally by using the test procedure SAEJ1269 or can be represented analytically with an expression like (Gillespie 1992)

$$C_{roll} = 0.05\ (1. + 0.01\ V). \quad (3)$$

In either case, at a given tire pressure, C_{roll} is a function of velocity. The resistance force due to the grade is,

$$F_{grade} = M\ g \sin \alpha, \quad (4)$$

and aerodynamic resistance is modeled as the pressure drag based on the frontal area of the vehicle, the vehicle drag coefficient, and dynamic pressure due to the velocity of the vehicle,

$$F_{aero} = 0.5\ C_d\ A\ \rho_{air}\ (V)^2, \quad (5)$$

where the frontal area is given by

$$A = 0.9\ H_a\ S_w. \quad (6)$$

The normal forces at the wheels are determined by taking moments about each wheel,

$$F_{nd} = (L_{nd}\ M\ g \cos \alpha - M\ dV/dt\ H_{cg} - Mg \sin \alpha\ H_{cg} - F_{aero}\ H_a) / L_w \quad (7)$$

$$F_{nnd} = (L_d\ M\ g \cos \alpha + M\ dV/dt\ H_{cg} + Mg \sin \alpha\ H_{cg} + F_{aero}\ H_a) / L_w. \quad (8)$$

Defining static weight distribution factors,

$$W_d = L_{nd} \cos \alpha / L_w \quad (9)$$

$$W_{nd} = Ld \cos \alpha / L_w \quad (10)$$

and the dynamic axle weight,

$$\Delta W_d = (M\ dV/dt\ H_{cg} + Mg \sin \alpha\ H_{cg} + F_{aero}\ H_a) / L_w \quad (11)$$

the normal reactions can be simplified,

$$F_{nd} = W_d\ M\ g - \Delta W_d \quad \text{(front wheel drive)} \quad (12)$$

$$= W_d\ M\ g + \Delta W_d \quad \text{(rear wheel drive)}$$

$$F_{nnd} = W_{nd}\ M\ g + \Delta W_d \quad \text{(front wheel drive)} \quad (13)$$

$$= W_{nd}\ M\ g - \Delta W_d \quad \text{(rear wheel drive)}$$

The relationship between the powertrain and the driving force at the wheels, F_d, is developed next, followed by detailed explicit models of each of the powertrain components.

Powertrain Relationships

The principal behavior variables characterizing a powertrain are torque and speed throughout the components. In analyzing a vehicle's performance, these behavior variables take on various values that constitute a vector of states as the vehicle analysis is conducted: states through a driving cycle, states when the engine is at maximum torque, and states effected by steady state criteria imposed on the vehicle. In the development of the powertrain relationships, the FDT partitions, and the coordination strategy, torque and speed are treated as only two behavior variables in contrast to representing every state separately. Other potential methods of representing state variables are discussed in the concluding remarks.

Figure 5 illustrates the power flow through the powertrain. The expressions relating engine torque, T_e, to torque at the driving wheel, T_d, are given by Equations (14) - (17).

$$T_i = T_e - T_{acc} - (\pi / 30)\,(I_e + I_{acc} + I_i)\, dN_e/dt \qquad (14)$$

$$T_{gb} = T_i\, R_t - (\pi /30)\, I_t\, dN_t/dt \qquad (15)$$

$$T_{fd} = T_{gb}\, \eta_{gb}\, \xi_{gb} - T_{ch} - (\pi /30)\,(I_{gb} + I_{ds})\, dN_{ds}/dt \qquad (16)$$

$$T_d = T_{fd}\, \eta_{fd}\, \xi_{fd} - (\pi /30)\, I_{fd}\, dN_d/dt \qquad (17)$$

These equations define the states (torque and speed) of each element in the powertrain at any point in time. Two additional state equations are required to define the relationship between engine actuation (throttle or manifold pressure) and driving force at the road. The first is given as part of the engine model development; the second is given with the wheel model. Development of the functional dependence of component efficiencies, and reduction ratios on geometric and control variables will complete the model development.

Wheels

The geometric wheel variable of interest is the effective tire radius, r_e. The principal behavior variables of interest are the adhesion coefficient μ_o, the traction coefficient μ, and the slip ratio S. These quantify the interaction at the tire-road interface by the expression

$$S = 1 - (\pi / 30)\, r_e\, N_d / V \,. \qquad (18)$$

The force that can be transmitted at the wheel without the wheel slipping (adhesion) is limited by the product of the normal force and the coefficient of adhesion. The wheel slips when the axle driving torque exceeds the adhesion torque according to

$$T_d / r_e > \mu_o\, F_{nd} \qquad (19)$$

and upon slip, the tractive force becomes,

$$F_d = F_{nd}\, \mu \qquad (20)$$

where F_{nd} is the normal force at the driving wheel. The adhesion coefficient, μ, depends on slip and tire material as shown in Figure 6. The traction coefficient is either experimentally determined (SAE Standard J1987) or represented analytically. Starkey et al. (1988) suggest the relation

$$\mu = 1.07\, \mu_o\, (1 - e^{-17.73\ S/(S-1)}) - 0.285\, S / (S-1). \qquad (21)$$

In either case, for partitioning considerations, the functional dependence remains unchanged. The entire behavior is explicitly represented by

$$F_d = F_{nd}\, \mu(S) + (1 - |\text{sign}\,(S)|\,)\,(T_d - (\pi / 30) I_d\, dN_{dr}/dt\,) / r_e \qquad (22)$$

where

$$\text{sign}(S) = \begin{cases} 1 & \text{for } S > 0 \\ -1 & \text{for } S < 0 \\ 0 & \text{for } S = 0. \end{cases}$$

Clearly, the driving force F_d is discontinuous. When adhesion is lost, the tractive force becomes zero, T_d accelerates the wheel, slip increases, μ increases with S, and maximum traction is regained.

The driveline is represented as a stiff shaft and speed reducer with the inertias, I_{ds}, I_{fd}, and the final drive ratio, ξ_{fd}, given in Appendix A. The relationship between drive shaft speed and wheel speed is

$$N_{ds} = \xi_{fd} N_d \quad (23)$$

$$dN_{ds}/dt = \xi_{fd} dN_d/dt \quad (24)$$

Transmission Relationships

The transmission geometric variables of interest are the number of gears, n_{gears}, and the gear ratios, ξ_{gbi}, i = 1, ..., n_{gears}. Behavior variables are the power conversion losses and control variables the gear states as functions of speed and torque. Two mechanisms contribute to transmission losses: rubbing friction between gears and energy dissipation in churning lubricating fluids. For powertrain analysis, losses are usually mapped as a function of gearbox speed and input shaft torque. The power conversion efficiency varies as a function of gearbox speed, input torque, and gear for the transmission of interest. The churning losses are represented similarly as a function of gearbox speed and gear.

Appendix B gives specific values but for decomposition analysis these losses are expressed implicitly as

$$\eta_{gb} = f(T_{gb}, N_t, i_{gear}) \quad (25)$$

$$T_{ch} = f(N_t, i_{gear}) \quad (26)$$

and the gearbox input speed is related to the drive shaft speed by

$$N_t = \xi_{gb} N_{ds} \quad (27)$$

$$dN_t/dt = \xi_{gb} dN_{ds}/dt. \quad (28)$$

A control problem exists in transmission design related to shifting strategies. The goal of the shift strategy is to keep the transmission in the gear closest to the best fuel consumption point without 'lugging' the engine at low speed and high torque and without frequent shifts that may annoy the driver. The shift strategy is usually specified as a function of shaft input speed, N_t, and some measure of engine load, namely, manifold pressure, p_i, engine torque, or a normalized load based on a calculated mass flow in the engine controller. For decomposition analysis the shift strategy is expressed implicitly as

$$i_{gear} = f(p_i, N_t). \quad (29)$$

More specific details of the shift strategy are given with the optimization results. The gearbox ratio is expressed implicitly,

$$\xi_{gb} = f(i_{gear}, \xi_1, \xi_2, \xi_3, ..., \xi_{ngears}). \quad (30)$$

The span of the gearbox is represented by the equality,

$$\xi_{span} = \xi_1 / \xi_{ngears}. \quad (31)$$

A Torque Converter Model

The torque converter developed originally for marine applications came into prevalence in passenger cars because of its benefits of torque multiplication, torsional damping, and efficient coupling at high speed ratios (Heldt 1955). The recent development of the lock-up clutch has improved its power conversion efficiency. The principles of converter operation are reviewed briefly in order to develop needed expressions. Jandasek (1988) provides a complete review of principles and design practices.

A single stage torque converter consists of three elements: an impeller, a stator, and a turbine shown in Figure 7. The important geometric variables are the torus diameter, D_t, the impeller design path diameter, D_i, the converter diameter, D_c, and the entrance and exit blade angles of the impeller, stator, and turbine.

Torque converters are characterized by the behavior variables torque ratio, R_t, and capacity factor, K,

$$R_t (R_S, R_{to}) = T_t / T_i \quad (32)$$

$$K (R_S, K_O) = N_i T_i^{-0.5} \quad (33)$$

which vary as a function of the ratio R_s of the turbine speed to the impeller speed,

$$R_s = N_t / N_i. \quad (34)$$

These important behavior variables are illustrated in Figure 8. When the turbine is held stationary and constant torque is applied to the impeller shaft causing impeller rotation, the converter is said

to be stalled ($R_S = 0$). Equation (33) defines a unique speed in terms of K_O. The stall speed, N_{stall}, is the speed at which the impeller rotates while the turbine is stalled. From Equation (33), the stall speed depends on the input torque and the capacity factor at $R_S = 0$, K_o , according to

$$N_{stall} = K_o \, T_i^{\,0.5} \, . \qquad (35)$$

The dominant design variables in converter design are D_C and the blade angle, α_i. Using functions in Eq. (33) and (34) as a base design, scaling laws can be developed. If similarity is maintained in the circuit path, while D_c is varied, the torque ratio curve remains virtually unchanged, but K-factor changes according to a similarity law, such as,

$$D_c'/ D_c = (K_O/K_O')^{0.4}. \qquad (36)$$

A smaller converter effects a higher K; a higher K implies a higher stall speed for a given input torque. Blade angles cause substantial change in both the torque ratio R_t and the K-factor, and a simple scaling factor can be used to represent the effect based on data presented in Jandasek (op. cit.), namely,

$$\alpha_t = (R_{to}' / R_{to}) \qquad (37)$$

$$K_o'/K_o = (\alpha_t)^{\,1.7}. \qquad (38)$$

The scaling factor, α_t, can then be used as a variable to design a new converter. It defines the K-factor, the torque ratio, and from Eq. (35) a new converter size can be determined according to

$$D_c'/ D_c = (\alpha_t)^{-.68} \qquad (39)$$

Equations (32)-(34) and (36)-(39) serve to define the torque converter.

Engine Model

The engine model is based on the model of Kuzak et al. (1984) but accounts for manifold tuning effects slightly differently. We use the friction model of Patton et al. (1989), include a simple NOx model, and account for effects of combustion stability degradation with burn duration.

The expression for torque is developed in terms of mean effective pressure, which is torque normalized against swept displacement volume. The expression for engine torque is

$$T_e = 7.955 \times 10^{-6} P_{bmep} \; b^2 \; s \, \pi / 4 \, n_c \qquad (40)$$

where P_{bmep} has units of bars. The brake mean effective pressure, P_{bmep}, is the difference between indicated mean effective pressure and friction mean effective pressure

$$P_{bmep} = P_{imep} - P_{fmep} \qquad (41)$$

The indicated mean effective pressure is the amount of fuel energy converted to indicated work normalized against displacement volume. It is given by the product of the mass of fuel, the lower heating value of the fuel, Q, the thermal efficiency of the engine cycle, η_t, and the air-to-fuel ratio, R_{af},

$$P_{imep} = 3.479 \times 10^{-2} \eta_t \, (p_{it} / T_m) \, Q / R_{af} \, . \qquad (42)$$

The thermal efficiency is expressed as

$$\eta_t = 0.9 \, (1 - c_r^{(-0.33 - .01 \, Regr/30)}) f_c - S_v \, (1500/N_e)^{0.5} \, (4.137/P_{imep})^{0.2} \qquad (43)$$

where

$$f_c = (1.18 - 0.18 \, \phi / 0.8) \qquad \phi \le 1$$

$$= (1.655 - 0.7 \, \phi) \qquad \phi > 1 \qquad (44)$$

$$S_v = 0.83 \, (12s + (c_r - 1)(6b + 4s)) / (b \, s \, (2 + c_r)). \qquad (45)$$

The 0.9 multiplier accounts for losses due to finite combustion times and is considered valid for displacements of 400 - 600 cc/cylinder and bore to stroke ratios of 0.8 - 1.2. The air-fuel correction factor, f_c, is based on the well-known effects of air-fuel ratio on idealized Otto cycles (Taylor, 1985). Heat transfer is strongly dependent upon surface-to-volume ratio. The S_v term is

the surface-to-volume ratio at a volume 1/3 of swept volume. About 50% of the heat loss in the Otto cycle occurs by that time in the thermodynamic cycle.

The breathing characteristics of a naturally aspirated engine depend on the ability of the fluid motion to follow the piston motion. The piston motion effects a rarefaction wave that propagates through the induction system to the throttle and results in an attendant compression wave which arrives at the intake valve. For engines with fixed geometry induction systems, the single torque peak occurs where the compression wave is 'tuned' to the runner lengths, cam events, and piston speed. For variable geometry induction systems, multiple torque peaks can be obtained. This tuning behavior is described with the Mach index, Z, the volumetric efficiency, η_v and the tuning pressure, Δp_t. These are, respectively, a normalized speed of sound, a normalized mass flow, and a scalar approximation to the effects of the compression wave.

The Mach index, defined as (Taylor, op cit.),

$$Z = 2 s N_e (b/d_i)^2 /(60 a_o C_s n_v) \qquad (46)$$

is the ratio of an idealized flow velocity past the valve to the speed of sound. The discharge coefficient, C_s, accounts for flow losses through the induction system and is expressed as

$$C_s = C_{stiff} C_m C_p (i_{vc} - i_{vo})/180 (C_m^2 + C_p^2 - C_m^2 C_p^2)^{-0.5} . \qquad (47)$$

The volumetric efficiency is the volume of air flow (referenced to standard conditions) normalized against the volume displaced by the piston. The tuning behavior is characterized by the volumetric efficiency curve as a function of Mach index and engine variables. It can be represented at various levels of detail. In the simplest approach, a baseline is determined and represented as function of Z,

$$\eta_v = f (Z). \qquad (48a)$$

As bore and stroke are changed the engine speed of the tuning peak changes accordingly. Such an approach only describes the relationship between piston speed and compressibility.

A straightforward and more detailed approach to account for induction and exhaust geometry is to use Helmholtz resonator theory (Engelman 1973) to locate the tuning peak as a function of runner length and diameter

$$\eta_v = f\,(L_{mi}, L_{me}, Z). \qquad (48b)$$

Jameson and Hodgins (1990) used this approach to successfully tune the induction and exhaust system for a Formula SAE competition engine; the result was a 34% improvement in torque over their base design. The limitation of Helmholtz theory is the inability to predict the change in amplitude of the volumetric efficiency at the peak. Empirical relationships for the amplitude change could be derived from experimental data like that given in Tabaczynski (1982).

One-dimensional compressible flow models are capable of predicting both the location and amplitude of the tuning peak. For the computational results presented in the last section of the article, an implementation of the model of Chapman et al. (op cit.) is used for Equation (48). For the coordination strategy developed in the article any of the three approaches could be used in an optimization study. For decomposition analysis volumetric efficiency is expressed implicitly as a function of engine speed, valve events, and manifold geometry as

$$\eta_v = f\,(\,i_{vo}, i_{vc}, e_{vo}, e_{vc}, i_{lift}, e_{lift}, n_v, L_{mi}, D_{mi}, L_{me}, D_{me}, Z) \qquad (48c).$$

The tuning effect is represented by a tuning pressure, Δp_t , which is added to the base manifold pressure to account for tuning,

$$p_{it} = p_i + \Delta p_t(\,Z)\,(p_i - 33.86)/(67.68) \qquad (49).$$

Parasitic losses of a naturally aspirated engine due to friction fall into five categories: pumping, bearing, piston-ring, valvetrain, and accessory friction. Expressions for pumping friction, bearing friction and piston-ring friction are taken from Patton et al. (1989) and are explained briefly. Accessory losses are scaled with displacement volume and power density.

Spark ignition engines use a throttle to control torque causing losses due to pressure drops. These losses are expressed in three terms of pressure drop across the throttle plate, across the

intake and exhaust valve, and across the exhaust system, respectively,

$$P_{fpu} = (P_a - p_{it}) + 4.12 \times 10^{-11} (p_{it}/P_{air})^2 ((N_e s b^2 / (30 n_v))^2 (d_i^{-4} + d_e^{-4}) + 0.178 \times 10^{-8} (p_{it}/P_{air})^2 (N_e s / 30)^2. \quad (50)$$

where P_a is the ambient pressure just upstream of the throttle.

The expression for bearing friction accounts for boundary lubrication in the main bearing seals, hydrodynamic friction in the main bearings, and pumping work for the lubricating fluids, corresponding to the three terms below

$$P_{fmb} = 1.22 \times 10^3 d_{bm}/(b^2 s n_c) + 3.03 \times 10^{-6} N_e d_{bm}^3 l_{bm} n_{bm}/(b^2 s n_c) + 1.35 \times 10^{-12} d_{bm}^2 N_e^2 n_{bm}/ n_c. \quad (51)$$

The expression for the rod/piston assembly accounts for rod bearing friction, rubbing friction of the piston skirt, piston-ring friction under no pressure loading and piston-ring friction due to loading from compression of the gas,

$$P_{fpr} = 3.03 \times 10^{-6} N_e d_{br}^3 l_{br} n_{br} /(b^2 s n_c) + 2.94 \times 10^{-3} N_e s / (30 b) + 4.06 \times 10^{2} (1 + 1000/ N_e) b^{-2} + 6.89 \times 10^{-2} p_i / P_{air} (0.088 c_r + 0.182 c_r^{(1.33 - 0.0238 Ne s /30000)}) \quad (52)$$

Valvetrains can be configured as pushrod or overhead cam and actuated with a rocker arm, a finger follower, or a direct acting bucket, and with sliding or rolling bearing elements. Valvetrain friction depends mostly on the mechanical configuration, so the valvetrain friction, P_{fvt}, is expressed as

$$P_{fvt} = 10 F_{spvt} d_i^2 / (b^2 s \pi /4) \quad (53)$$

where the specific valvetrain friction is a function of speed and valvetrain type. The values used in

the optimization study are given in Appendix B. For decomposition the specific valvetrain friction is represented implicitly as

$$F_{spvt} = f(v_{type}, N_e). \quad (54)$$

The friction mean effective pressure for the oil pump is computed by scaling with respect to displacement volume between two baseline designs according to

$$P_{foil} = (O_{ld}(N_e) - O_{hd}(N_e))\ (4.6 - b^2\ s\ \pi\ /4\ n_c\ x\ 10^{-6})/\ 2.7\ + O_{hd}(N_e) \quad (55)$$

where O_{ld} and O_{hd} are measured pumping losses for a 1.9L I-4 engine and a 4.6L V-8 respectively.

Similarly, the friction mean effective pressure for the water pump is computed by scaling relative to two baseline designs with respect to power density according to

$$P_{fh2o} = H_{lpd}(N_e) + (H_{hpd}(N_e) - H_{lpd}(N_e))(P_{bmep}(N_{pp})N_{pp}/895.2 - 54)/16. \quad (56)$$

H_{lpd} and H_{hpd} are the water pumping losses of two engines of low and high power density respectively. The values for O and H are given in Appendix B.

The total expression for friction is

$$P_{fmep} = P_{fpu} + P_{fpr} + P_{fmb} + P_{fvt} + P_{foil} + P_{fh2o}. \quad (57)$$

At a specified engine torque, speed, air-fuel ratio, and egr level, the fuel flow rate ($\dot{m}_f$) is the air flow rate ($\dot{m}_a$) divided by the air-fuel ratio. The air flow rate is simply the product of air density and volume displaced by the piston motion,

$$\dot{m}_f = \dot{m}_a / R_{af}$$

$$= 3.479\ x10^{-9}\ (p_i/T_m)\ N_e\ n_c\ b^2\ s\ \pi\ /(480\ R_{af}\ ). \quad (58)$$

In the practical control of an engine at a given engine speed, four degrees of freedom exist in obtaining a desired torque: manifold pressure, spark advance, air-fuel ratio, and exhaust gas recirculation (egr). The control strategy aims to operate the engine at the air-fuel ratio, egr, and spark advance values that minimize fuel consumption, meet emissions constraints and maintain

driveability. These values are stored in the engine microprocessor as a function of manifold pressure and engine speed. The conversion efficiency of the catalytic converter is maximum at stoichiometric air-fuel ratios, hence the air-fuel schedule tends to be stoichiometric in the region of the speed/load map where the emissions are regulated. The fuel enrichment at high loads reduces exhaust temperatures within temperature limits of the catalytic converter and exhaust valves.

The egr strategy can be varied by scaling its amplitude with a multiplier F_{egr}. Again, explicit values are given in Appendix B and for decomposition analysis the control strategies can be represented implicitly as the simple functions

$$R_{af} = f\,(p_i, N_e) \qquad (59)$$

$$R_{egr} = f\,(p_i, N_e, F_{egr}) \qquad (60)$$

The relationships developed so far assume the engine is operating at minimum spark timing for best fuel consumption (MBT). Strategies deviating from MBT spark timing are beyond the scope of the present model.

The burn duration calculation follows directly from the expressions for ignition delay, τ_{ig}, and energy release, τ_{er}, given in Hires et al. (1978) (Equations (30) and (32) of their article),

$$\theta_{0\text{-}90} = 6\, N_e\, (\tau_{ig} + \tau_{er}) \qquad (61a)$$

The expressions are functions of chamber height, viscosity, piston speed, laminar flame speed, and bore. The expression for laminar flame speed is given explicitly in Heywood (1984). To preclude unduly biasing the FDT with combustion model detail, for decomposition analysis, burn duration is represented as

$$\theta_{0\text{-}90} = F(N_e, b, s, R_{resf}, R_{af}, p_i, T_m) \qquad (61b).$$

A correlation of NOx emissions has been developed with the form

$$\dot{m}_{nox} = C_{nox}\, 50\, e^{(-R_{resf} * 12.88)}\, 7.955 \times 10^{-6}\, P_{imep} b^2 s\, \pi /4\, n_c N_e /7122 \qquad (62)$$

where C_{nox} is a calibration coefficient between 0.5 and 1.0.

Various accessories are driven off the engine that reduce vehicle performance and fuel economy. Appendix B gives the included accessories: front-end accessory drive belt, oil pump on the transmission, and alternator. The air conditioning compressor and power steering pump are not considered. For decomposition analysis, the accessories are considered implicitly by the relation

$$T_{acc} = f(N_e). \tag{63}$$

The final expressions for the engine model development are

$$T_m = (310+400\, R_{egr}) / (1 + R_{egr}/100). \tag{64}$$

$$R_{resf} = f(R_{egr}, p_i). \tag{65}$$

At a given engine torque and speed, fuel consumption decreases monotonically with gas-fuel ratio up to the combustion stability limit. Increased residual fraction, increased air-fuel ratio or both can increase gas-fuel ratio. Excessive gas-fuel ratio results in unstable combustion causing an increase in fuel consumption and emissions. This increase occurs at a 0-90 burn time of about 70^o. A representation of this stability limit is constructed empirically, by using the asymptotic K-S function (Kreisselmeier and Steinhauser 1979).

This concludes the engine model development.

3 OPTIMIZATION MODEL

The remaining task is to develop equations for the system criteria. The metro-highway fuel economy is defined as the integrated fuel flow over the city and highway cycles,

$$MPG_{m\text{-}h} = \left\{ \rho_f \left[\frac{0.55}{7.45} \int_{city} \dot{m}_f \, dt + \frac{0.45}{10.25} \int_{hwy} \dot{m}_f \, dt \right] \right\}^{-1} \tag{66}$$

The integrated value of NOx over the cycle is modeled as a discretized integral

$$NOx = \int_{cycle} \dot{m}_{nox} \, \eta_{cat} dt \tag{67}$$

The acceleration criteria are computed from solution of Equations (68)-(70).

$$\tau_{0\text{-}60} = \tau : \int_0^{\tau} \frac{dV}{dt}\, dt = 60 \text{ mph; initial conditions: } V_o = 0 \quad (68)$$

$$\tau_{5\text{-}20} = \tau : \int_0^{\tau} \frac{dV}{dt}\, dt = 20 \text{ mph; initial conditions: } V_o = 5 \text{ mph} \quad (69)$$

$$S_{0\text{-}4} = \int_0^4 \left(\int_0^4 \frac{dV}{dt} dt \right) dt \text{ ; initial conditions: } V_o = 0. \quad (70)$$

Computationally, each integral is discretized into sums where the integrand is computed for each discrete time interval, Δt_i. For decompositon analysis, Δt_i can be viewed as a state variable, and in the original formulation of this problem (Wagner 1993) it was considered in the FDT. However, in the final implementation of a numerical integration scheme, it becomes a parameter in the sense that it is prescribed by the integration scheme, and hence neglected in the construction of the FDT. This treatment of the time parameter, makes partitioning results obtained with heuristic search methods directly comparable to those obtained with global search methods.

The gradeability criteria are defined by steady-state formulations of the equations of motion. Rearrangement yields the following expressions

$$\sin \alpha_s = (T_e(60\, \xi_{fd}\, \xi_1 V_s/(2\, r_e\, \pi))\, \xi_{fd}\, \xi_1\, \eta_{fd}\eta_{gb}\, R_{to} - r_e\, (F_{roll} + F_{aero}))\, (r_e\, M\, g)^{-1} \quad (71)$$

and

$$\sin (\alpha_c) = (T_e(60\, \xi_{fd}\, \xi_{ngears\text{-}1}\, V_c/(2\, r_e\, \pi))\, \xi_{fd}\, \xi_{ngears\text{-}1}\, \eta_{fd}\eta_{gb} - r_e\, (F_{roll} + F_{aero}))\, (r_e\, M\, g)^{-1} \quad (72)$$

where, $\alpha_c = 3.43^o$ (6% grade) and $V_s = 5$ mph.

Equations (1) through (72) define the functional relationships among the variables describing the system. Formulation of the optimal design problem by identifying objective function and constraints follows.

The objective is to develop a vehicle that competes in a given market, meets emissions requirements, and has the maximum fuel economy possible. Target acceleration characteristics are specified to deem it competitive in its market. The U.S. Federal Clean Air Act constrains the NOx emissions to no more than 0.4 g/mile; time to accelerate from 0 to 60 mph is no greater than the

target, τ_o; time to accelerate from 5 to 20 mph is no greater than the target, τ_1; distance traveled in four seconds is no less than the target distance, S_{base}; starting gradeability is no less than 30%; cruising velocity at grade is no less than 65 mph. These are given as the first six inequality constraints,

$$g_1: NOx/0.4 - 1 \leq 0$$
$$g_2: \tau_{0\text{-}60}/\tau_o - 1 \leq 0$$
$$g_3: \tau_{5\text{-}20}/\tau_1 - 1 \leq 0$$
$$g_4: S_{base}/S_{0\text{-}4} - 1 \leq 0$$
$$g_5: 30/\alpha_s - 1 \leq 0$$
$$g_6: 65 / V_c - 1 \leq 0$$

Baseline acceleration criteria, τ_o, τ_1, S_{base} are given in Appendix B.

In addition there are several operating constraints which must be satisfied. First, the gear states are constrained such that the powertrain does not lug. A given power requirement of the engine can be satisfied by several torque-speed pairs dependent on the gear ratio. If an engine operates at a high torque and very low speed the vibration modes of the engine are more easily sensed by the driver because they are lower frequency and higher amplitude. Under such conditions, the powertrain is said to lug. The constraint is imposed by specifying an upper bound on T_e as a function of gear and speed. These constraints are subjective and validated experimentally (see Appendix B). For decomposition analysis a single function is used

$$g_7: T_e(N_e)/T_{emax}(N_e) - 1 \leq 0. \qquad (73)$$

There are several operating constraints on the engine. It must not knock and it must always operate in the stable combustion regime. An expression for knock limited bore is

$$g_8: c_r - 13.2 + 0.045\, b \leq 0. \qquad (74)$$

Combustion stability is maintained by always constraining the burn duration to less than 70^o

$$g_9: \theta_{0-90}/\ 70 - 1 \leq 0. \qquad (75)$$

If the combustion model were not included, a comparable constraint would be to constrain egr such that it does not exceed some value at a specified speed and load.

There are also several geometric constraints. First, in passenger cars the geometry of the final drive usually constrains the final drive ratio (Bosch 1986) to

$$g_{10},\ g_{11}\colon\ 2. \le \xi_{fd} \le 5. \qquad (76)$$

The gear ratios are characterized by the step down ratios, $\xi_{i+1} / \xi_{i.}$ If the step down is too large a smooth shift is difficult to attain. Liberal constraints for a four speed transmission are

$$g_{12},\ g_{13}\colon\ 1.6 \le \xi_1 / \xi_2 \le 2 \qquad (77)$$

$$g_{14},\ g_{15}\colon\ 1.2 \le \xi_2 / \xi_3 \le 1.5 \qquad (78)$$

At this point it is convenient to assume the example value of $n_{gears} = 4$. For a planetary gear set, at least one gear should be direct drive, hence,

$$\xi_3 = 1$$

and lastly, the span of a set of planetaries is usually

$$g_{16},\ g_{17}\colon\ n_{gears} - 0.5 \le \xi_1 / \xi_{ngears} \le n_{gears} + 0.5 \qquad (79)$$

Current design practice for nearly all conventional spark ignition engines constrains the bore-to-stroke ratios and displacement per cylinder according to

$$g_{18},\ g_{19}\colon\qquad 0.8 \le\ b/s\ \le 1.2 \qquad (80)$$

$$g_{20},\ g_{21}\colon\qquad 400 \le \pi\, b^2 s/\,(4\, n_c)\ \text{x}\ 10^{-3} \le 600. \qquad (81)$$

The ratio of combined valve diameters to the bore and the ratio of exhaust to intake valve diameter are constrained according to

$$g_{22}\colon\ d_i + d_e\ - 0.88\ b \le 0 \qquad (82)$$

$$g_{23},\ g_{24}\colon\ \ 0.85 \le d_e/d_i \le .89. \qquad (83)$$

Bearing dimensions scale with bore size where the scaling factor depends on engine configuration as given in Appendix B.

$$h_1\colon\qquad d_{bm}\ /b =\ K_{dm} \qquad (84)$$

$$h_2\colon\qquad l_{bm}\ /\ b =\ K_{lm} \qquad (85)$$

$$h_3\colon\qquad d_{br}\ /\ b\ =\ K_{dr} \qquad (86)$$

$$h_4\colon\qquad l_{br}\ /\ b\ \ =\ K_{lr} \qquad (87)$$

Regarding valve timing, a number of design limitations exist for the valvetrain to function successfully. First the events are bounded so they occur in the appropriate region of the thermodynamic cycle. Second, the difference,

$$g_{25}: (i_{vo} - e_{vc}) / 50 - 1.0 \leq 0 \qquad (88)$$

is bounded to preclude excessive residual fraction at idle conditions. Third, limits exist on the valvetrain acceleration. For both intake and exhaust cams, the acceleration is defined as the second derivative of the lift profile as a function of cam angle and expressed in units of cm/deg^2. For decomposition analysis purposes they are expressed as

$$g_{26}: \; -.008 \leq acc_{iv} (i_{vo}, i_{vc,} i_{lift}) \leq 0.011 \qquad (89)$$

$$g_{27}: \; -.008 \leq acc_{ev} (e_{vo,} e_{vc,} e_{lift}) \leq 0.011 \qquad (90)$$

The specific bounds depend on the valvetrain type, -0.008 and 0.011 correspond to the pushrod valvetrain used in the example.

Appendix A summarizes the complete model as presented. Defining equations are treated as zero-valued equalities and each function is given a unique name and number. These identifiers are used in annotating the FDT and corresponding adjacency matrices of the optimization model. The optimal design problem statement is then as follows.

maximize	MPG_{m-h}	Metro-highway fuel economy
subject to		
g_1:	$NOx/0.4 - 1 \leq 0$	CAA driven constraint on NOx
g_2:	$\tau_{0-60}/\tau_o - 1 \leq 0$	0-60 mph time; τ_o = 11.0 sec
g_3:	$\tau_{5-20}/\tau_1 - 1 \leq 0$	5-20 mph time; τ_1 = 1.81 sec.
g_4:	$S_{base} / S_{0-4} - 1 \leq 0$	Launch distance; S_{base}=88.4 ft.
g_5:	$30.0 / \alpha_s - 1 \leq 0$	Starting gradability ($\geq$ than 30%)
g_6:	$65 / V_c - 1 \leq 0$	Cruising velocity ($\geq$ 65 mph @ 6% grade)
g_7:	$T_e(N_e)/T_{emax}(N_e) - 1 \leq 0$	Lugging limits
g_8:	$c_r - 13.2 + 0.045\, b \leq 0$	Knock limited bore
g_9:	$\theta_{0-90} / 70 - 1 \leq 0$	Combustion stability constraint
g_{10}:	$2. - \xi_{fd} \leq 0$	Final drive ratio constraint
g_{11}:	$\xi_{fd} - 5 \leq 0$	Final drive ratio constraint
g_{12}:	$1.6 - \xi_1 / \xi_2 \leq 0$	Step down ratio constraint

g_{13}:	$\xi_1 / \xi_2 - 2.0 \leq 0$	Step down ratio constraint	
g_{14}:	$1.2 - \xi_2 / \xi_3 \leq 0$	Step down ratio constraint	
g_{15}:	$\xi_2 / \xi_3 - 1.6 \leq 0$	Step down ratio constraint	
g_{16}:	$n_{gears} - 0.5 - \xi_1 / \xi_{ngears} \leq 0$	Gear span constraint	
g_{17}:	$\xi_1 / \xi_{ngears} - n_{gears} - 0.5 \leq 0$	Gear span constraint	
g_{18}:	$0.8 - b/s \leq 0$	Bore-stroke ratio constraint	
g_{19}:	$b/s - 1.2 \leq 0$	Bore-stroke ratio constraint	
g_{20}:	$400 - \pi b^2 s/ (4 n_c) \times 10^{-3} \leq 0$	Displacement/cylinder constraint	
g_{21}:	$\pi b^2 s/ (4 n_c) \times 10^{-3} - 600 \leq 0$	Displacement/cylinder constraint	
g_{22}:	$d_i + d_e - 0.88 b \leq 0$	Valve size constraint	
g_{23}:	$0.85 - d_e/d_i \leq 0$	Valve size constraint	
g_{24}:	$d_e/d_i - 0.87 \leq 0$	Valve size constraint	(91)
g_{25}:	$(i_{vo} - e_{vc}) / 50 - 1.0 \leq 0$	Valve event constraint	
g_{26}:	$acc_{iv} (i_{vo}, i_{vc}, i_{lift}) - K_{acci} \leq 0$	Valve acceleration constraint	
g_{27}:	$acc_{ev} (e_{vo}, e_{vc}, e_{lift}) - K_{acce} \leq 0$	Vavle acceleration constraint	
h_1:	$d_{bm} /b - K_{dm} = 0$	Main bearing diameter constraint	
h_2:	$l_{bm} / b - K_{lm} = 0$	Main bearing length constraint	
h_3:	$d_{br} / b - K_{dr} = 0$	Rod bearing diameter constraint	
h_4:	$l_{br} / b - K_{lr} = 0$	Rod bearing diameter constraint	
h_{5+i}:	$i = 0, ..., 56$	Defining model equations	

4 PARTITIONING

The FDT of the optimization model and its undirected graph (adjacency matrix) are shown in Figure 9. Partition metrics include: (i) preference for a feasible coordination strategy which implies a search for linking variables, (ii) at least two disjoint partitions having at least 20 functions each, (iii) the smallest number of linking variables (but not to exceed ten). The heuristic search scheme for acceptable partitions is:

1) Rank variables according to the number of times each appears in the FDT, initialize counters i and j to 1.
2) Construct a vector of linking variables, $\mathbf{y}_i$, starting with the first highest ranked variable.
3) Delete $\mathbf{y}_i$ from FDT, perform depth-first-search on the graph of the modified FDT, and test partitions against acceptability criteria.
4) If acceptable, store $\mathbf{y}_i$ as a candidate vector to be enumerated.

5) If the number of variables in $\mathbf{y}_i$ is less than the upper bound, create $\mathbf{y}_{i+1}$ by appending the next highest ranked variable to $\mathbf{y}_i$ and go to 3. Otherwise continue.

6) For each stored candidate vector, construct an additional set of candidate vectors, $\mathbf{y}_{ij}$, (j=1,.., e) by combinatorial enumeration of the set of variables in the candidate vector. Perform step 3 on each vector $\mathbf{y}_{ij}$ (j=1,.., e). From those vectors with acceptable partitions select the one having the smallest number of linking variables.

The first set of disjoint partitions satisfying the acceptability criteria is found with linking variables $\mathbf{y} = (T_e, F_{aero}, p_i, M, s, b, N_e)$. Subsequent enumeration reveals that $\mathbf{y} = (T_e, N_e, p_i)$ gives the relatively balanced set of partitions in the FDT shown in Figure 10. Specification of engine torque, T_e and engine speed, N_e corresponds to a 'cut' at the crankshaft; specification of manifold pressure, p_i, 'cuts' the engine relations from the transmission shift strategy which is specified as a function of manifold pressure. This partition is then accepted for coordination. Interestingly, Michelena and Papalambros (1995) using spectral partitioning obtained a bisection of this problem with one additional linking variable (the accessory torque), while Krishnamachari (1996) using integer programming with more relaxed constraints on relative size found the same partition as the heuristic search. The quality of the partition ultimately must be assessed by the suitability of an attendant coordination strategy. We now proceed to develop a coordination strategy based on the above partitions.

5 COORDINATION STRATEGY DEVELOPMENT

The partition can be described generically as follows,

Linking Variables		
$\mathbf{y} = (T_e, N_e, p_i)$		Engine torque, engine speed, manifold pressure
Partition 1 (Engine relations)		
$\mathbf{x}_1$		Engine variables
$f(\mathbf{y}, \mathbf{x}_1)$		Objective, dependent only on $\mathbf{y}$ and $\mathbf{x}_1$
$\mathbf{h}_1(\mathbf{y}, \mathbf{x}_1)$	$= \mathbf{0}$	Defining equations dependent on linking variables, $\mathbf{y}$, and $\mathbf{x}_1$
$\mathbf{h}_1(\mathbf{x}_1) = \mathbf{0}$		Defining equations dependent only on $\mathbf{x}_1$
$\mathbf{g}_1(\mathbf{y}, \mathbf{x}_1)$	$\leq \mathbf{0}$	Constraints dependent on linking variables, $\mathbf{y}$, and $\mathbf{x}_1$
$\mathbf{g}_1(\mathbf{x}_1) \leq \mathbf{0}$		Constraints dependent only on $\mathbf{x}_1$
Partition 2 (Driveline relations)		

$\mathbf{x}_2$		Driveline/vehicle variables
$\mathbf{h}_2(\mathbf{y}, \mathbf{x}_2)$	$= \mathbf{0}$	Defining equations dependent on linking variables, $\mathbf{y}$, and $\mathbf{x}_2$
$\mathbf{h}_2(\mathbf{x}_2) = \mathbf{0}$		Defining equations dependent only on $\mathbf{x}_2$
$\mathbf{g}_2(\mathbf{y}, \mathbf{x}_2)$	$\leq \mathbf{0}$	Constraints dependent on linking variables, $\mathbf{y}$, and $\mathbf{x}_2$
$\mathbf{g}_2(\mathbf{x}_2) \leq \mathbf{0}$		Constraints dependent only on $\mathbf{x}_2$

and the generic hierarchical coordination strategy appropriate for this partition may be represented as follows.

Master Problem		Subproblems (i = 1, 2)		
$\min_{\mathbf{y}} \; f(\mathbf{y}, \mathbf{x}^*(\mathbf{y}))$		$\min_{\mathbf{x}_i} \; f(\mathbf{y}^*, \mathbf{x}_i)$		
s.to: $\mathbf{h}_y(\mathbf{y}) = \mathbf{0}$		$\Rightarrow$ s.to: $\mathbf{h}_i(\mathbf{y}^*, \mathbf{x}_i) = \mathbf{0}$		
$\mathbf{g}_y(\mathbf{y}) \leq \mathbf{0}$		$\mathbf{y}^*$ $\mathbf{h}_i(\mathbf{x}_i) = \mathbf{0}$		
$\mathbf{h}_i(\mathbf{y}, \mathbf{x}_i^*(\mathbf{y})) = \mathbf{0}$		$\mathbf{g}_i(\mathbf{y}^*, \mathbf{x}_i) \leq \mathbf{0}$		(92)
$\mathbf{h}_i(\mathbf{x}_i^*(\mathbf{y})) = \mathbf{0}$		$\Leftarrow$ $\mathbf{g}_i(\mathbf{x}_i) \leq \mathbf{0}$		
$\mathbf{g}_i(\mathbf{y}, \mathbf{x}_i^*(\mathbf{y})) \leq \mathbf{0}$		$\mathbf{x}^*(\mathbf{y})$ i = 1, 2		
$\mathbf{g}_i(\mathbf{x}_i^*(\mathbf{y})) \leq \mathbf{0}$				
i = 1, 2				

The challenge is to develop a suitable approximation of $\mathbf{x}^*(\mathbf{y})$. If the linking variables are geometric variables a gradient-based linear approximation or one based on parametric sensitivity analysis could be constructed. However, the linking variables are state variables (engine torque, engine speed, and manifold pressure) which take on discrete values as they are computed over their respective driving cycles. The fuel economy cycle of 1372 seconds implies at least as many discrete values of torque and speed to integrate the fuel flow over the cycle. Similarly, numerical integration of the performance constraints implies discrete values of torque and speed. A gradient-based approximation of $\mathbf{x}^*(\mathbf{y})$ would imply 1372 representations of the geometric variables in $\mathbf{x}_1$ to be represented in the master problem, a burdensome strategy at best. Moreover, the physical significance of the sensitivity of geometric variables to state variables is unclear. One might suggest a coordination strategy like those used in trajectory problems but such strategies are applied when the optimal variables sought are control variables explicitly dependent on the state variables. In the system model here, geometric and control variables were intentionally included to effect a problem of sufficient scope. This issue arises because we have made no aspect

decomposition prior to examining the FDT; control, state, and geometric variables have been included in the model, the FDT, and the partitioning.

We examine another strategy that addresses the physical significance of the sensitivity of geometric variables to torque and speed. The key approximations of interest are the behavior variables for fuel flow, ($f(\mathbf{y}, \mathbf{x}_1)$), NOx, ($\mathbf{g}_1(\mathbf{y}, \mathbf{x}_1)$) and acceleration calculations, ($\mathbf{g}_2(\mathbf{y}, \mathbf{x}_2)$) because they depend on linking variables and local variables. The challenge is to accommodate torque, speed, and manifold pressure between the master problem and the subproblem.

When comparing engines of different displacement, it is common practice (Taylor 1985) to compare torques normalized by displacement (bmep) and to compare flow rates normalized by power (specific consumption) at equal bmep. With the same reasoning, displacement can be used to scale engine behavior. We introduce engine displacement as a single variable, V_d; the subscripts 'y' and '1' indicate values of V_d in the master problem and subproblem, respectively. We introduce the equality

$$V_{d1} = n_c \pi b^2 s/4 \tag{93}$$

to hold displacement fixed in the subproblem and the equality

$$\frac{T_{ey}}{V_{dy}} = \frac{T_{e1}}{V_{d1}} \tag{94}$$

to scale engine torque with displacement. This facilitates approximations for $f(\mathbf{y}, \mathbf{x}_1(\mathbf{y}))$ and $g_1(\mathbf{y}, \mathbf{x}_1(\mathbf{y}))$ with the following relationships:

$$f(\mathbf{y}, \mathbf{x}_1(\mathbf{y})) = \sum_{i=1}^{N} \dot{m}_f (T_{ey}, N_e) = \sum_{i=1}^{N} \dot{m}_f (T_{e1}, N_e) \frac{V_{dy}}{V_{d1}} \tag{95}$$

$$g_1(\mathbf{y}, \mathbf{x}_1(\mathbf{y})) = \sum_{i=1}^{N} \dot{m}_{NOx} (T_{ey}, N_e) \eta_{cat} = \sum_{i=1}^{N} \dot{m}_{NOx} (T_{e1}, N_e) \frac{V_{dy}}{V_{d1}} \eta_{cat} \tag{96}$$

These approximations allow us to formulate the coordination strategy given below.

Master Problem

$$
\begin{aligned}
\min_{\mathbf{y}\ \mathbf{x}_2} \quad & f(\mathbf{y}, \mathbf{V_d}) \\
\text{s.to:} \quad & \mathbf{h}_y(\mathbf{y}) = \mathbf{0} \\
& \mathbf{g}_y(\mathbf{y}) \le \mathbf{0} \\
& \mathbf{h}_1(\mathbf{y}, \mathbf{x}_1^*(\mathbf{y})) = \mathbf{0} \\
& \mathbf{h}_1(\mathbf{x}_1^*(\mathbf{y})) = \mathbf{0} \\
& \mathbf{h}_2(\mathbf{y}, \mathbf{x}_2) \le \mathbf{0} \\
& \mathbf{h}_2(\mathbf{x}_2) \le \mathbf{0} \\
& \mathbf{g}_1(\mathbf{y}, \mathbf{x}_1^*(\mathbf{y})) = \mathbf{0} \\
& \mathbf{g}_1(\mathbf{x}_1^*(\mathbf{y})) = \mathbf{0} \\
& \mathbf{g}_2(\mathbf{y}, \mathbf{x}_2) \le \mathbf{0} \\
& \mathbf{g}_2(\mathbf{x}_2) \le \mathbf{0}
\end{aligned}
$$

$$
\begin{aligned}
& \mathbf{T}_{ey}^*, \mathbf{N}_{ey}^*, V_{dy} \\
& \Rightarrow \\
& \Leftarrow \\
& V_{d1}^* \\
& f^*(\mathbf{T}_{e1}, \mathbf{N}_e) \\
& g_1^*(\mathbf{T}_{e1}, \mathbf{N}_e)) \\
& \mathbf{p}_i(\mathbf{T}_e, \mathbf{N}_e) \\
& \mathbf{T}_{e1w}, \mathbf{N}_{ew}
\end{aligned}
$$

Subproblem

$$
\begin{aligned}
\min_{\mathbf{x}\ i} \quad & f(\mathbf{y}^*, \mathbf{x}_1) \\
\text{s.to:} \quad & \mathbf{h}_1(\mathbf{y}^*, \mathbf{x}_1) = \mathbf{0} \\
& \mathbf{h}_1(\mathbf{x}_1) = \mathbf{0} \\
& V_{d1} - n_c \pi b^2 s/4 = 0 \\
& \mathbf{g}_1(\mathbf{y}^*, \mathbf{x}_1) \le \mathbf{0} \\
& \mathbf{g}_1(\mathbf{x}_1) \le \mathbf{0}
\end{aligned}
$$

.

(97)

The master problem (MP) is formulated in $\mathbf{y}$ and since the objective does not depend on $\mathbf{x}_2$, the MP can be constructed in terms of $\mathbf{y}$ and $\mathbf{x}_2$. The subproblem, which solves for $\mathbf{x}_1$, corresponds to the engine. Equation (93) is introduced into the subproblem (SP) as an equality constraint that holds engine displacement fixed during optimization in the SP; Eq. (94) is used in the MP to scale engine torque with displacement; Eq. (95) and (96) scale fuel flow and emissions with discplacement. The physical significance of this coordniation is that the effects of engine geometry detail are ignored in the master problem and captured only in the subproblem.

Coordination Strategy

1. Initialization. Initialize all design variables. Construct table of fuel flow, emissions flow, and manifold pressure map as a function of torque and speed. Construct wide-open-torque curve as a function of speed.
2. Solve MP to find optimal $\mathbf{y}^*$, $\mathbf{x}_2^*$, and V_{yd}^* .
3. Solve SP to find optimal $\mathbf{x}_1^*$.
4. If $\| \mathbf{x}^k - \mathbf{x}^{k-1} \| \le \varepsilon$ stop; otherwise increment *k* and return to 2.

Initial tests with the strategy had difficulty returning a WOT torque curve that maintained feasibility of the performance constraints when returning to the master problem. In minimizing fuel economy, the subproblem would return low bore-stroke ratios which lowered the speed at

peak torque and lowered peak power. For this reason, two additional constraints were added to the subproblem that bound engine torque at the torque converter stall speed,

$$g_{28}: 1 - \frac{T_e(N_{stall})}{T_e^k(N_{stall}^k)} \leq 0 \tag{98}$$

and at peak power,

$$g_{29}: 1 - \frac{T_e(N_{pp})\, V_d\, N_{pp}}{T_e^k(N_{pp}^k)\, V_d^k\, N_{pp}^k} \leq 0 \tag{99}$$

In effect, this coordination strategy is now a partial minimization strategy that maintains feasibility through reduced complexity approximations. The master problem partially minimizes fuel economy as a function of master problem variables, $\mathbf{y}$, and $\mathbf{x}_2$, and approximates engine effects with a single scaling variable, the engine displacement. The engine subproblem partially minimizes fuel economy as a function of engine variables, $\mathbf{x}_1$, and approximates vehicle constraints with requirements for peak power and torque at stall speed.

The vehicle relations (Partition 2) are computed with a proprietary vehicle simulation code based originally on the work of Blumberg (1976) and Mencik et al. (1978). The code can be configured to both receive fuel and emissions maps and report the necessary speed/load points for the metro-highway cycle. A transmission shift strategy can be specified or an optimal strategy sought. For the results presented below, optimal shifting was sought with constraints on upshifts, downshifts, and lugging speeds (g_7) and time in gear (Wagner and Papalambros 1996). For the performance calculations the shift strategy was specified to upshift at maximum vehicle acceleration.

The engine relations are solved with two software tools working in sequence. The first, a one-dimensional compressible flow model (Chapman et al. 1982) provides volumetric efficiency and the second (Kuzak et al. 1984) solves for the remaining relations. Each of these programs, accompanied with appropriate interfaces to an optimizer (Wagner 1991, Wagner 1993, Tzannetakis 1994) facilitated implementing the coordination strategy. Some initial results with the strategy are presented next.

6 COORDINATED OPTIMIZATION SOLUTION

Assume a vehicle segment has been selected with the acceleration targets 0-60 time τ_0 = 11.0 sec, 5-20 time τ_1 = 1.81 sec, four second distance S_{base} = 88.4 ft. Assume body and chassis decisions have yielded the vehicle parametervalues given in the appendix. This leaves as variables the engine geometry and egr schedule, $\mathbf{x}_1$ = (b, s, c_r, d_i, d_e, L_{mi}, D_{mi}, L_{me}, D_{me} i_{vo}, i_{vc}, e_{vo}, e_{vc}, d_{bm}, l_{bm}, d_{br}, l_{br}, i_{lift}, $e_{lift,}$ F_{egr}), and transmission gears and torque converter size, $\mathbf{x}_2$ = (ξ_1, ξ_2, ξ_3, ξ_4, ξ_{fd}, ξ_{span}, α_t,i_{gear}) to be optimized. The coordination strategy begins by solving for all initial values in SP to create a starting point for MP (a map of fuel flow, NOx emissions, and manifold pressure as a function of engine speed and torque based on the initial engine design, and a wide-open throttle torque curve).

Table I summarizes the results of the strategy. The first column identifies geometric and behavior variables in the MP and SP; the second lists the variable name; the third gives the units. The initial values of the variables of interest (geometric and behavior) are given in the fourth column. The next seven columns give results as the strategy sequences through optimization in the MP and SP. Note that the final point of MP defines the displacement of the engine in the initial point of SP. Similarly, the final point of SP defines the fuel flow and emissions used in MP.

The coordination strategy converged in two overall iterations and improved the fuel economy by 10.8% (3 mi/gal) relative to the baseline powertrain. At the feasible starting point, (column IV) none of the acceleration constraints are active: $\tau_{0\text{-}60,}$ $\tau_{5\text{-}20,}$ and S_{base} are within the bounds by 0.7 seconds, 0.1 seconds, and 4.0 feet respectively. In the solution to the first iteration of MP (column V), the step-down ratio ξ_1/ξ_2 is reduced, the final drive ratio is nearly unchanged, the size factor on the torque converter α_t, is increased, the engine is down-sized by 8%, and the gear box span is increased by 0.1 ratios. First gear ratio ξ_1 is reduced by 20%; the second ξ_2 by 10%; and the fourth ξ_4 by 18%. The active constraints are the 0-60 time $\tau_{0\text{-}60}$ and the bound on the torque converter scaling factor α_t. The fuel economy is improved by 7.9%. Gradeability criteria are virtually unaffected.

Essentially, the optimizer reduced engine displacement and gear ratios until the acceleration constraint on $\tau_{0\text{-}60}$ became active. Fuel economy improvements are primarily the result of engine displacement reduction, and also the result of reduced overdrive (ξ_4) and increased torque amplification in scaling the torque converter with α_t. The increased α_t also improves converter efficiency, resulting in a lower engine idle torque which provides better city fuel economy. The reduced overdrive effects better highway fuel economy.

The reduction of ξ_1 is not intuitive. The 0-60 time is primarily a function of first gear, so a reduction in first gear ratio should compromise performance. However, the increased torque ratio in the torque converter offsets this effect. The reduced step-down ratio also enhances performance; it enables the engine to operate closer to its peak power point during the WOT acceleration. The reduced step-down ratio is also beneficial for shift quality. The higher K in the torque converter effects a higher stall speed. The engine will wind to higher speed on acceleration and the perceptible driveability of such a system remains to be determined. Conventional powertrains have a nominal stall speed between 1900 and 2200 rpm and stall speed was not constrained in this formulation.

The starting point for SP (col. VI) lies on several boundaries; the intake valve constraint is active and the constraint on compression ratio is actually exceeded. The cam timing of the baseline engine is based on a production cam which had undergone several production iterations. The cam is considered constraint bound in terms of acceleration, overlap, and events. It remained unchanged. However, an improved manifold was obtained as shown in Figure 11. By increasing the intake runner length and increasing the runner diameters, a substantial improvement in volumetric efficiency was obtained at higher engine speeds. Some of the improvement was at the expense of volumetric efficiency at 3000 rpm; however, no performance was compromised at the stall speed of 2721. The improved volumetric efficiency resulted in margin for a more favorable bore-stroke ratio for fuel economy. The lower bore-stroke ratio reduced the speed of peak power yet the net power remained unchanged from the starting point of this iteration. The solution to SP

reduces fuel flow by 1.3%; the constraint on peak power, the constraint on compression ratio, and the constraint on burn duration are active. The combustion stability constraint limited the egr factor to 1.37. The change in egr and the change in bore-stroke ratio (from 1.11 to 1.04) both result in better thermal efficiency and lower fuel flow. The bore-stroke ratio could change because of the latitude in the peak power constraint which was the result of an improved manifold. The improved volumetric efficiency allowed this change.

The first solution to SP was then used to generate a new fuel, emissions, and torque curve to solve the MP. The results of this optimization are shown in columns VIII and IX of Table I. In this iteration small changes were observed in the gear ratios, but the engine was downsized by 5% effecting another 2% in fuel economy improvement. Again, the 0-60 constraint became active. In this iteration, fuel economy was improved at the expense of 0-60 time until the 0-60 constraint became active. Note the reduction in stall speed from 2728 to 2655 caused by the reduced torque from engine down-sizing. Also, NOx is reduced 15%, the 5-20 time is virtually the same, and only 3 mph has been sacrificed in cruising gradeability velocity compared to the original baseline.

A second set of optimal torque-speed points were generated to solve the second iteration of SP (column X). In this iteration no improvement in the objective was obtained. Not a surprising result, since the starting point is at the peak power constraint boundary, and changes in bore-stroke only improve the power at the expense of fuel. Similarly, the starting point is on the burn rate boundary, and egr will improve fuel only at the expense of burn rate.

Figure 12 summarizes the iteration history of the master problem, and illustrates the fuel economy/performance tradeoff as a function of engine displacement. In both iterations the 0-60 starts feasible, and the engine is downsized until the 0-60 constraint is active. The improvement in volumetric efficiency by varying the manifold geometry allowed an additional 5% reduction in engine displacement which resulted in an additional 2% improvement in metro-highway fuel

economy. The coordination strategy demonstrates the significant effect a single subsystem can have on the overall system.

7 CONCLUSIONS

Decomposition analysis was applied to a significant vehicle design problem. A model was presented for computing vehicle fuel economy, acceleration, and gradeability criteria. The FDT was constructed and partitioned using metrics appropriate for feasible decomposition methods. The minimum linking variables that allowed decomposition were engine torque, engine speed, and manifold pressure. A coordination strategy was developed to determine an optimal set of geometric and control variables to maximize fuel economy subject to performance constraints. The strategy converged quickly, primarily because approximations of subproblem coupling facilitated a feasible starting point for the master problem in each iteration. This case study showed that automated partition techniques must be coupled with carefully selected coordination strategies for an overall advantageous system optimization study.

ACKNOWLEDGMENT

This research was partially supported by a University Research Grant from Ford Motor Company and by the Automotive Research Center at the University of Michigan, a US Army Center of Excellence in Modeling and Simulation of Ground Vehicles, under Contract No. DAAE07-94-C-R094. This support is gratefully acknowledged. The authors are also grateful to Mr. Brad Boyer, Mr. Dave Brigham, Mr. Rich Belaire, Dr. Jim Novak, and Mr. Nick Tzannetakis for useful insights on the nuances of modeling drivelines, torque converters, engines, and induction systems respectively.

REFERENCES

Altus, S., Kroo, I., and Gage, P., "A Genetic Algorithm for Scheduling and Decomposition of Multidisciplinary Design Problems", *ASME Paper No. 95-141*, Boston, MA.

Assanis, D.N., and Polishak, M. 1989, "Valve Event Optimization in a Spark Ignition Engine", *ASME Transactions, Internal Combustion Engines*, Vol. 9, pp201-208.

Auiler, J.E., Zbrozek, J.D., Blumberg, P.N., 1977, "Optimization of Automotive Engine Calibration for Better Fuel Economy - Methods and Applications", *SAE Paper No. 770076*, Warrendale, Pennsylvania.

Balling, R. and Sobieszczanski-Sobieski, J. 1994, "Optimization of Coupled Systems: A Critical Overview of Approaches", in *Proceedings of 5th AIAA/NASA/USAF/ISSMO Symposium on Multidisciplinary Analysis and Optimization*, Panama City, 1994, pp. 753-773.

Blumberg, P.N. (1976) "Powertrain Simulation: A Tool for the Design and Evaluation of Engine Control Strategies in Vehicles", *SAE Paper No. 760518*, Warrendale, PA.

Bosch Automotive Handbook, 1986, Robert Bosch GmbH, Stuttgart.

Cramer, E., Dennis, J., Frank, P., Lewis, R., and Shubin, G., "Problem Formulation for Multidisciplinary Optimization", *SIAM Journal of Optimization*, Vol. 4, No. 4, pp. 754-776.

Chapman, M., Novak, J. M., and Stein, R. A. (1982) "Numerical Modeling of Inlet and Exhaust Flows in Multi-cylinder Internal Combustion Engines", *Proceedings of the ASME Winter Annual Meeting, Flows in Internal Combustion Engines*, ed. T. Uzkan, Phoenix, AZ, November 14-19.

Davis, G.C., and Borgnakke, C., 1982,"The Effect of In-Cylinder Flow Processes (Swirl, Squish, and Turbulence Intensity) on Engine Efficiency - Model Predictions", *SAE Transactions*, Paper No. 820045, Warrendale, PA.

Davis, G.C., Mikulec, A., Kent, J.C., and Tabaczynski, R.J., 1986, "Modeling the Effect of Swirl on Turbulence Intensity and Burn Rate in S. I. Engines and Comparison with Experiment", *SAE Paper No. 860325*, Warrendale, PA.

Davis, G.C., and Tabaczynski, R.J., 1988, "The Effect of Inlet Velocity Distribution and Magnitude on In-Cylinder Turbulence Intensity and Burn Rate - Model vs. Experiment", *Journal of Engineering for Gas Turbines and Power*, Vol. 110, pp 509-514.

Donner, A.R. (1978) "Optimal Control Solution of the Automotive Emission-Constrained Minimum Fuel Problem", PhD Dissertation, Dept. of Computer, Information and Control Enginneering, University of Michigan, Ann Arbor.

Engelman, H.W., 1973, "Design of a Tuned Intake Manifold", ASME Paper 73-WA/DGP-2.

Gillespie, T.D., 1992, *Fundamentals of Vehicle Dynamics*, SAE, Warrendale, PA.

Heldt, P.M., 1955, *Torque Converters or Transmissions*, Chilton Co., Philadelphia.

Hendrickson, B. and Leland, R., 1993, "The Chaco User's Guide, Version 1.0", *Technical Report SAND93_2339*, Sandia National Laboratory, Albequerque, New Mexico.

Heywood, J.B., 1984, "Combustion Chamber Design for Optimum Spark-Ignition Engine Performanc", Presented at teh International Association of Vehicle Design Congress, Geneva, Switzerland, Feb. 22-24.

Hires, S.D., Tabaczynski, R.J, and Novak, J.M., 1978 "The Prediction of Ignition Delay aand Combustion, Intervals for a Homogeneous Charge, Spark Ignition Engine", *SAE Paper 780232* Warrendale, Pennsylvania.

Hock, W., and Schittkowski, K., 1981, "Test Examples for Nonlinear Programming Codes", Test Problem No. 104, *Lecture Notes in Economics and Mathematical Systems, No. 187*, (ed.) M. Beckman and H.P.Kunzi, Springer-Verlag, Berlin.

Jameson, R.T., and Hodgins, P.A., 1990, "Improvement of Torque Charasteristics of a Small, High Speed Engine through the Design of Helmholtz-Tuned Manifolding", *SAE Paper 900680*, Warrendale, PA.

Jandasek, V.J., 1988, "Design of Single Stage, Three Element Torque Converter", *Design Practices: Passenger Car Automatic Transmissions,2nd Edition*, Vol. 5, ed. N.F. Avery, SAE, Warrendale, PA.

Kreisselmeier, G., and Steinhauser, R., 1979, "Systematic Control Design by Optimizing a Vector Performance Index", *Proceedings of the IFAC Symposium on Computer Aided Design of Control Systems*, Zurich, Switzerland, pp. 113-117.

Krishnamachari, R. (1996) *A Decomposition Synthesis Methodology for Optimal Systems Design*, Doctoral Dissertation, Dept. of Mechanical Engineering, The University of Michigan, Ann Arbor.

Krishnamachari, R., and Papalambros, P. (1996) "Optimal Hierarchical Decomposition Synthesis Using Integer Programming", *Proc. 1996 Design Automation Conf.*, Irvine, CA.

Kuzak, D.M., Belaire, R.C., Le, S., and Brigham, D.R. (1984) "Parametric Simulation of the Fuel Consumption Effects of Engine Design Variation with Advanced Transmission Powertrains", *SAE Paper No. 841243*, SAE Passenger Car Meeting, Dearborn, MI, October 1-4.

Lamancusa, J.S. (1988) "Geometric Optimization of Internal Combustion Induction Systems for Minimum Noise Transmission", *Journal of Sound and Vibration,* Vol. 127, No.2, pp 303-318.

Mencik, Z., Tobler, W.E., and Blumberg, P.N. (1978) "Simulation of Wide Open Throttle Vehicle Performance", *SAE Paper No. 780289*, Warrendale, PA.

Michelena, N. and Papalambros, P. (1994) " A Network Reliability Approach to Optimal Decomposition of Design Problems", *Advances in Design Automation,-1994*, B.J. Gilmore (ed.), Vol.2, ASME, New York, pp. 195-204.

Michelena, N. and Papalambros, P. (1995) "Optimal Model-based Decomposition of Powertrain System Design", Transactions of ASME, *Journal of Mechanical Design*, 117(4):499-505.

Newman, C. E., Stein, R. A., Warren, C. C. and Davis, G. C. (1989) "The Effects of Load Control with Port Throttling at Idle - Measurements and Analyses", *SAE Paper No. 890679*, Warrendale, PA.

Niste, K., 1989, "Gear Shift Optimization", *Automotive Simulation: Proceedings of the 2nd Engineering Cars/Trucks Simulation Symposium*, Schlieree Germany, ed. Moshe R. Heller, Springer-Verlag, pp. 49-60.

Patton, K.J., Nitschke, R.G., and Heywood, J.B., 1989, "Development and Evaluation of a Friction Model for Spark-Ignition Engines", *SAE Paper No. 890836,* Warrendale, PA.

Rishavy, E.A., Hamilton, S.C., Ayers, J.A., and Keane, M.A., 1977, "Engine Control Optimization for Best Fuel Economy with Emission Constraints", *SAE Paper No. 770075*, Warrendale, PA.

Rogers, J.L., 1989, "A Knowledge Based Tool for Multi-level Decomposition of a Complex Design Problem", *NASA TP 2903*, Langley Research Center, Hampton, VA.

Rogers, J. and Bloebaum, C., "Ordering Design Tasks Based on Coupling Strengths", in *Proceedings of 5th AIAA/NASA/USAF/ISSMO Symposium on Multidisciplinary Analysis and Optimization,* Panama City, 1994, pp. 708-717.

Sakamoto, H., Kiyoto, S., Tokimori, S. (1992) "Study on Torque Converter Circuit Profile", *SAE Paper 920765*, Warrendale, PA.

Starkey, J. M., Gray, S., and Watts, D. (1988) "Vehicle Performance Simulation and Optimization Including Tire Slip", *SAE Paper 881733*, Warrendale, PA.

Tabaczynski, R.J., 1982, "Effects of Inlet and Exhaust System Design on Engine Performance", *SAE Paper 821577*, Warrendale, Pennsylvania.

Taylor, C.F. (1985) *The Internal Combustion Engine in Theory and Practice: Vol. 1 & Vol. II. Second Ed., Revised,* MIT Press, Cambridge.

Tzannetakis, N., Jensen, M., and Novak, J. (1994) "Development of Optimal Design Methodologies for Engine Air Management", *15th International Symposium on Mathematical Programming*, Ann Arbor, MI.

Wagner, T.C. (1993) *A General Decomposition Methodology for Optimal System Design,* PhD Dissertation, Dept. of Mechanical Engineering, University of Michigan, Ann Arbor.

Wagner, T.C., and Papalambros, P. (1991) "Optimal Engine Design Using Nonlinear Programming and the Engine System Assessment Model", Technical Report No. SR-91-154, Ford Motor Co., Dearborn, MI.

Wagner, T.C., and Papalambros, P. (1993a)"A General Framework for Decomposition Analysis in Optimal Design", in *Advances in Design Automation - 1993*, B.J. Gilmore, ed. vol.2, New York, ASME, pp. 315-325.

Wagner, T.C., and Papalambros, P. (1993b) "Implementation of Decomposition Analysis in Optimal Design", in *Advances in Design Automation - 1993*, B.J. Gilmore, ed. vol.2, New York, ASME, pp. 327-335.

Wagner, T.C., and Papalambros, P. (1996), "Decomposition Analysis of an Automotive Powertrain Design Problem: Model Development, Partitioning, and Optimization", *University of Michigan MEAMTechnical Report No. 96XXXX,* Ann Arbor, MI. (Available on website http://arc.engin.umich.edu/...htl)

Wismer, D. A.(ed.), 1971, *Optimization Methods for Large Scale Systems,* McGraw-Hill Book Company, New York, NY.

Wismer D.A, and Chattergy, R., 1978, *Introduction to Non-linear Optimization: A Problem Solving Approach*, North-Holland, New York, NY

Woodard, J. K., Johnson, G. E., and Lott, R. L. (1989) "Automated Design of a Turbocharged, Fueled, Four-stroke, Engine for Minimum Fuel Consumption", *ASME Journal of Mechanisms, Transmissions, and Automation in Design Automation*, Vol. 11., pp. 389-394.

MODEL -BASED DECOMPOSITION

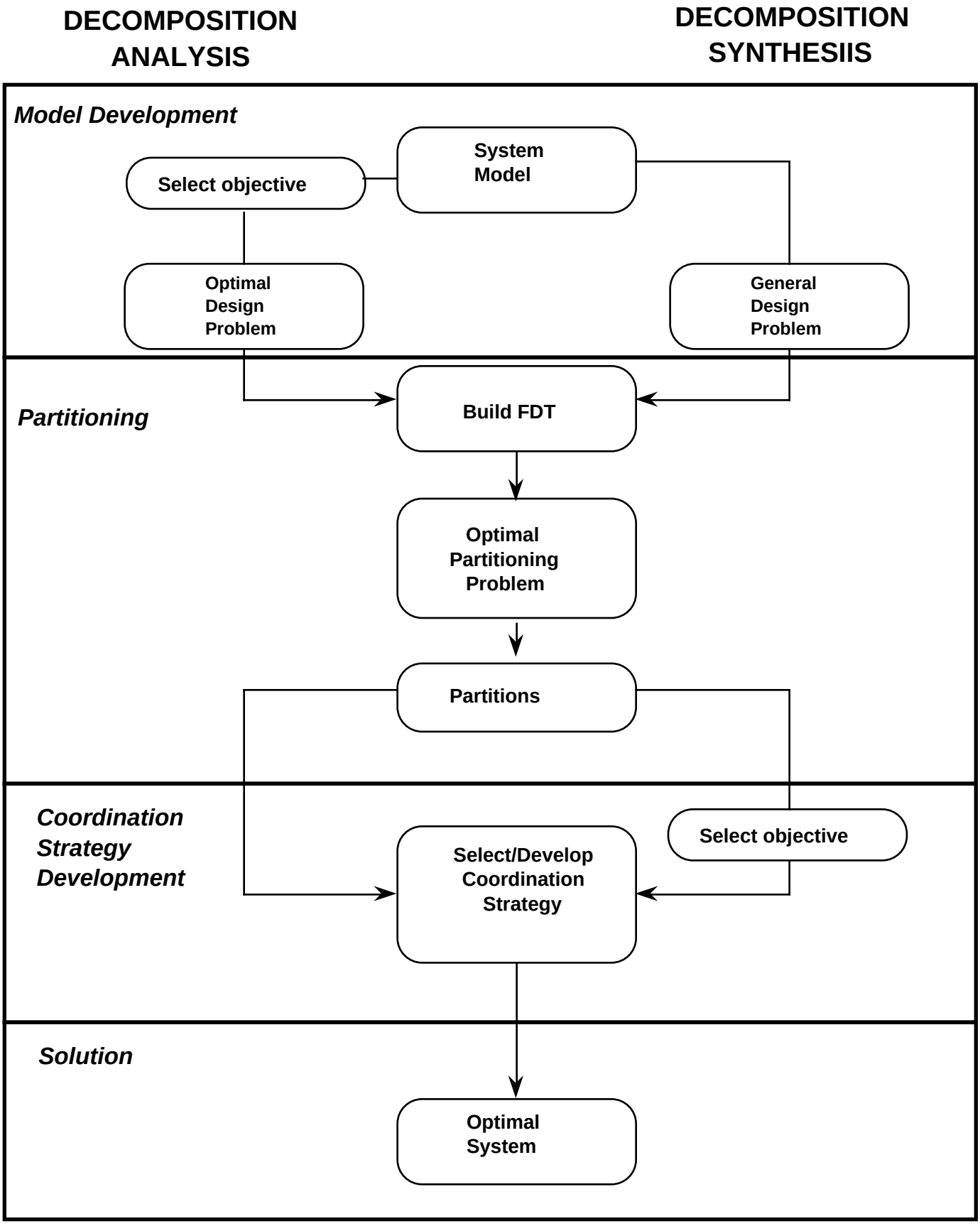

Figure 1. The Model-Based Decomposition Methodology

NLP PROBLEM **FDT**

		Expressions
Objective	f_1	$0.4\ x_1^{0.67}\ x_7^{-0.67}$
	f_2	$0.4\ x_2^{0.67} x_8^{-0.67}$
	f_3	$10 - x_1$
	f_4	x_2
Constraints	g_1	$0.1\ x_1 + 0.0588\ x_5\ x_7 - 1.0$
	g_2	$0.1\ x_1 + 0.1\ x_2 + 0.0588\ x_6\ x_8 - 1.0$
	g_3	$4x_3x_5^{-1} + 2x_3^{-0.71}\ x_5^{-1} + 0.0588\ x_3^{-1.3}x_7 - 1.0$
	g_4	$4x_4x_6^{-1} + 2x_4^{-0.71}\ x_6^{-1} + 0.0588\ x_4^{-1.3}x_8 - 1.0$
Bounds	g_{i+4}	$-0.1 - x_i,\ \ i = 1, ..., 8$
	g_{i+12}	$x_i - 10,\ \ i = 1, ..., 8$

	x_1	x_2	x_3	x_4	x_5	x_6	x_7	x_8
f_1	1						1	
f_2		1						1
f_3	1							
f_4		1						
g_1	1				1		1	
g_2	1	1				1		1
g_3			1		1		1	
g_4				1		1		1

PARTITIONS **PARTITIONED FDT**

DP_y	$\mathbf{y} = (x_1);\ f(\mathbf{y}) = (f_3);\ \mathbf{g}(\mathbf{y}) = (g_5, g_{13})$
DP_1	$\mathbf{x}_1 = (x_2, x_4, x_6, x_8);\ \mathbf{f}_1(\mathbf{y},\mathbf{x}_1) = ();\ f_1(\mathbf{x}_1) = f_2 + f_4$
	$\mathbf{g}_1(\mathbf{y},\mathbf{x}_1) = (g_2)$
	$\mathbf{g}_1(\mathbf{x}_1) = (g_4)$
	$\mathbf{g}_b(\mathbf{x}_1) = (g_6, g_8, g_{10}, g_{12}, g_{14}, g_{16}, g_{18}, g_{20})$
DP_2	$\mathbf{x}_2 = (x_3, x_5, x_7);\ \mathbf{f}_2(\mathbf{y},\mathbf{x}_2) = (f_1);\ f_2(\mathbf{x}_2) = ()$
	$\mathbf{g}_2(\mathbf{y},\mathbf{x}_2) = (g_1);\ \mathbf{g}_2(\mathbf{x}_2) = (g_3)$
	$\mathbf{g}_b(\mathbf{x}_2) = (g_7, g_9, g_{11}, g_{15}, g_{17}, g_{19})$

	x_1	x_2	x_4	x_6	x_8	x_3	x_5	x_7
f_3	1							
f_2		1			1			
f_4		1						
g_2	1	1		1	1			
g_4			1	1	1			
f_1	1							1
g_1	1						1	1
g_3						1	1	1

Figure 2. Partitioning example of an NLP problem.

Master Problem		Subproblem (i = 1, ..., p)
$\min_{\mathbf{y}\ \mathbf{x}_i}$ $f(\mathbf{y}, \mathbf{x}^*(\mathbf{y}))$ s.to: $\mathbf{h}_y(\mathbf{y}) = \mathbf{0}$ $\mathbf{g}_y(\mathbf{y}) \le \mathbf{0}$ $\mathbf{h}_i(\mathbf{y}, \mathbf{x}_i^*(\mathbf{y})) = \mathbf{0}$ $\mathbf{h}_i(\mathbf{x}_i^*(\mathbf{y})) = \mathbf{0}$ $\mathbf{g}_i(\mathbf{y}, \mathbf{x}_i^*(\mathbf{y})) \le \mathbf{0}$ $\mathbf{g}_i(\mathbf{x}_i^*(\mathbf{y})) \le \mathbf{0}$	$\Rightarrow$ $\mathbf{y}^*$ $\Leftarrow$ $\mathbf{x}^*(\mathbf{y})$	$\min_{\mathbf{x}_i}$ $f(\mathbf{y}^*, \mathbf{x}_i)$ s.to: $\mathbf{h}_i(\mathbf{y}^*, \mathbf{x}_i) = \mathbf{0}$ $\mathbf{h}_i(\mathbf{x}_i) = \mathbf{0}$ $\mathbf{g}_i(\mathbf{y}^*, \mathbf{x}_i) \le \mathbf{0}$ $\mathbf{g}_i(\mathbf{x}_i) \le \mathbf{0}$ i = 1,...,p

Figure 3. Generic Coordination Strategy for Problem Structure.

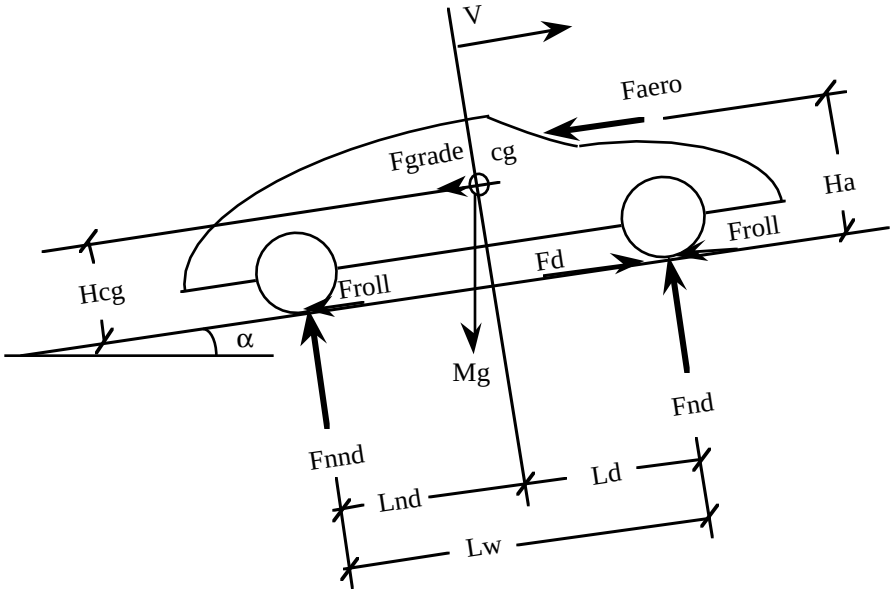

Figure 4. Body forces acting on vehicle.

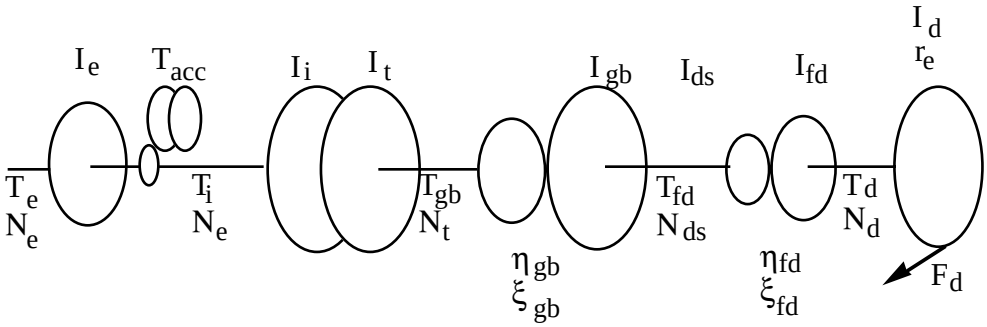

Figure 5. Schematic of power flow through the powertrain.

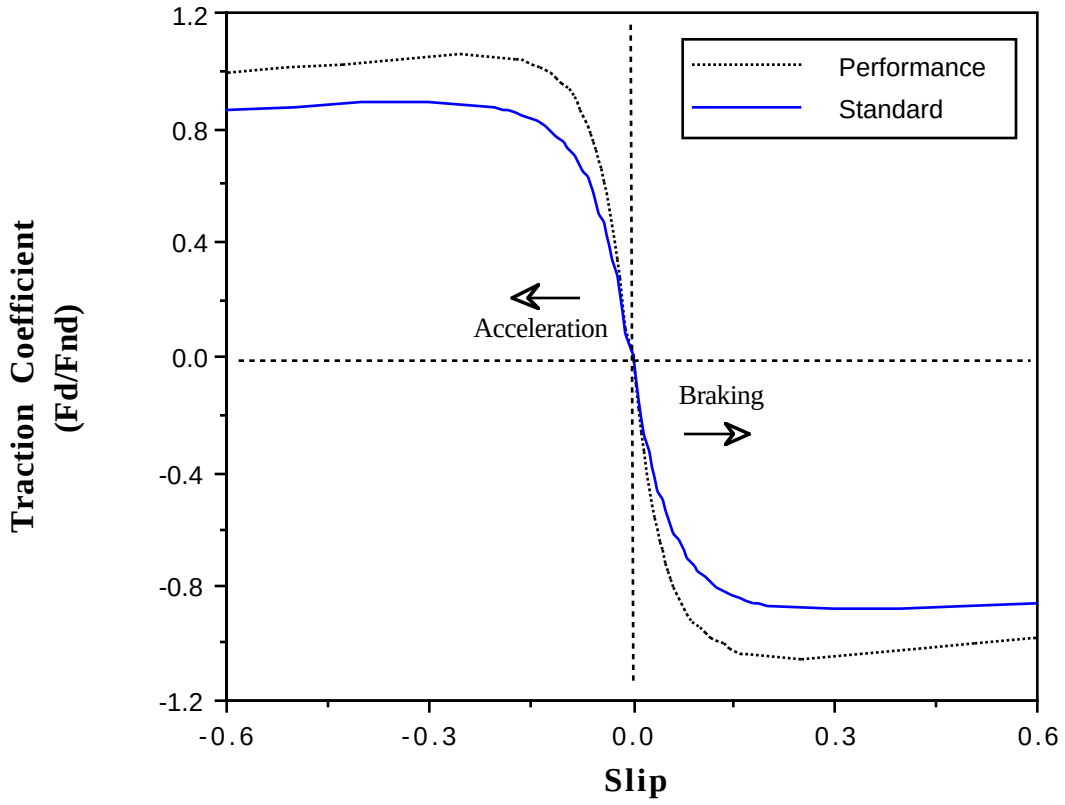

Figure 6. Traction coefficients, μ(S), as a function of slip for two radial tires.

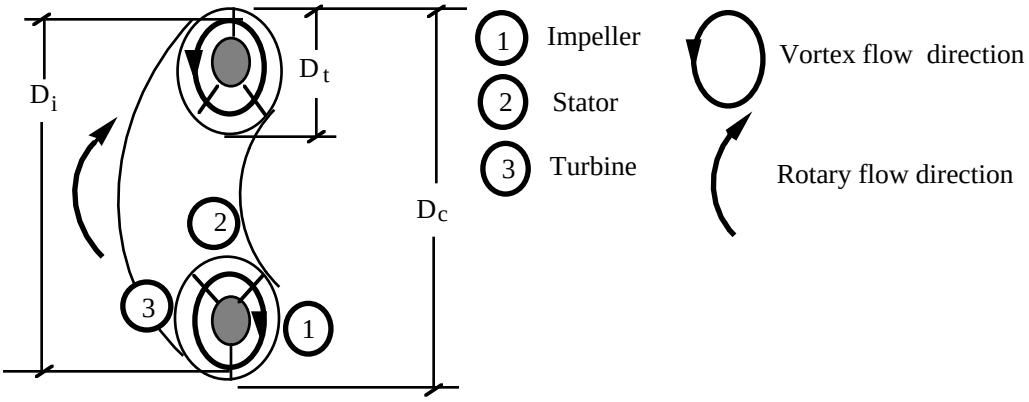

Figure 7. Cross section of torque converter torus showing oil flow path

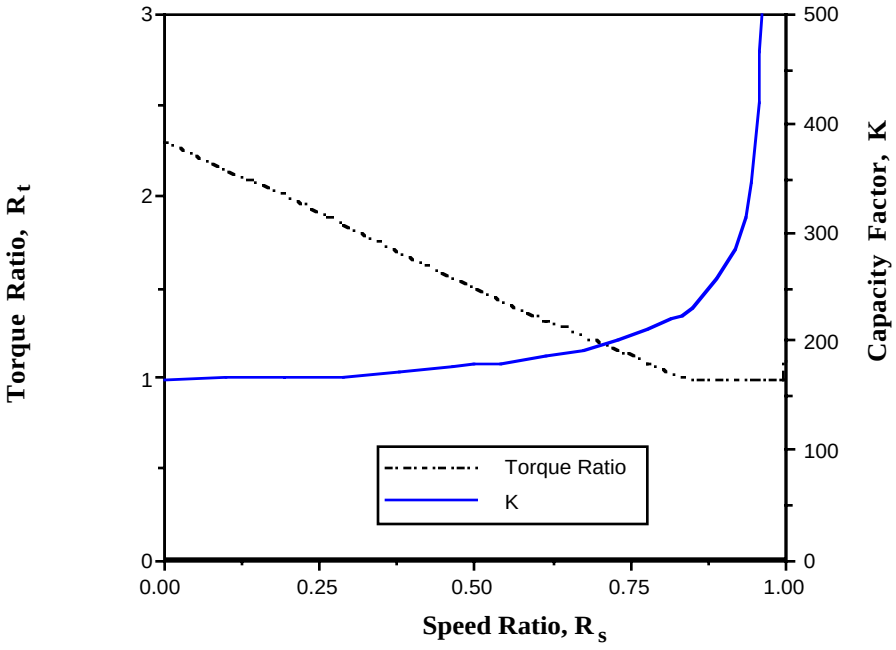

Figure 8. Typical performance curves of a three stage torque converter.

Functional Dependence Table **Graph (Adjacency Matrix) of FDT**

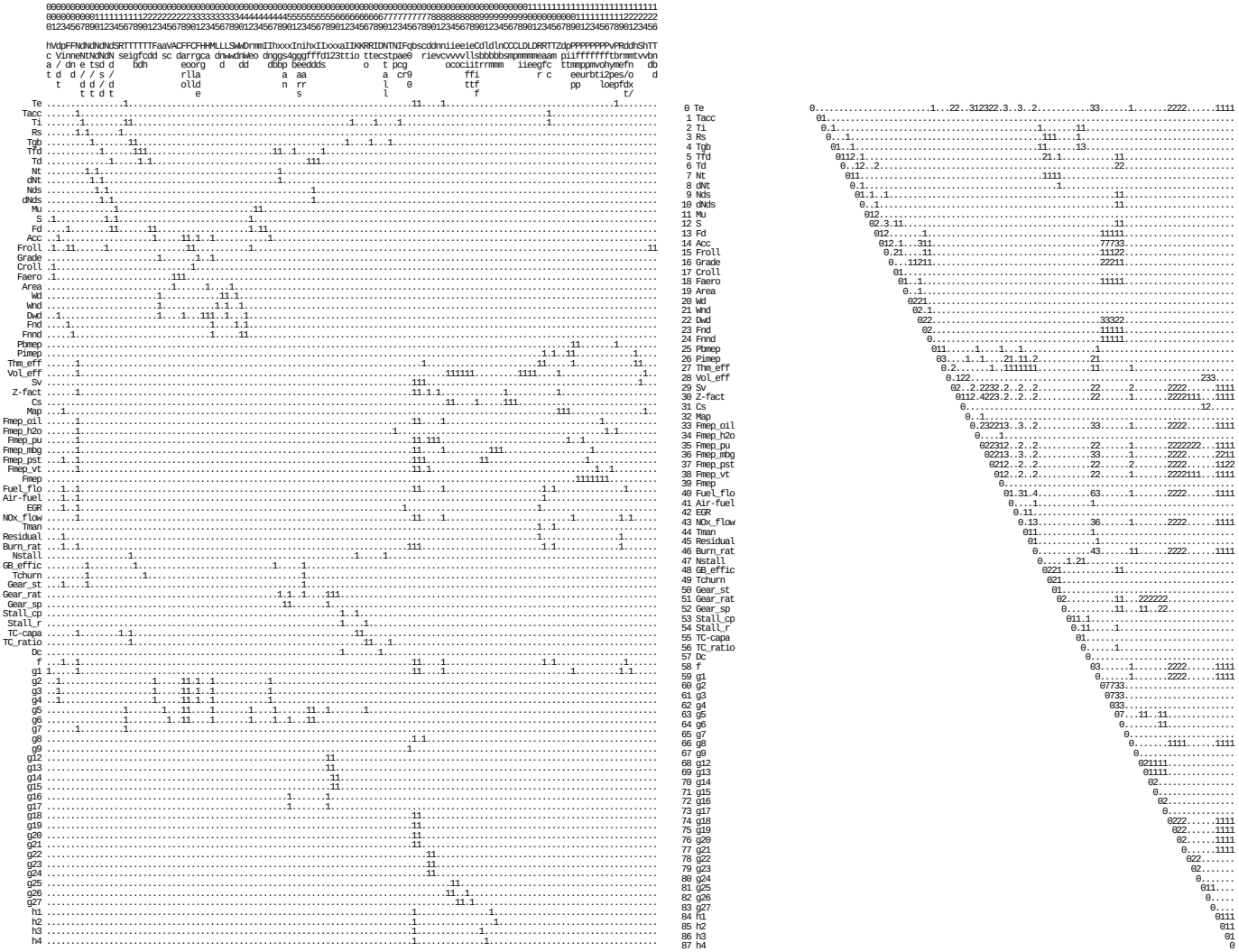

Figure 9. FDT and graph of FDT for vehicle design problem.

Partitioned Graph **Resultant FDT**

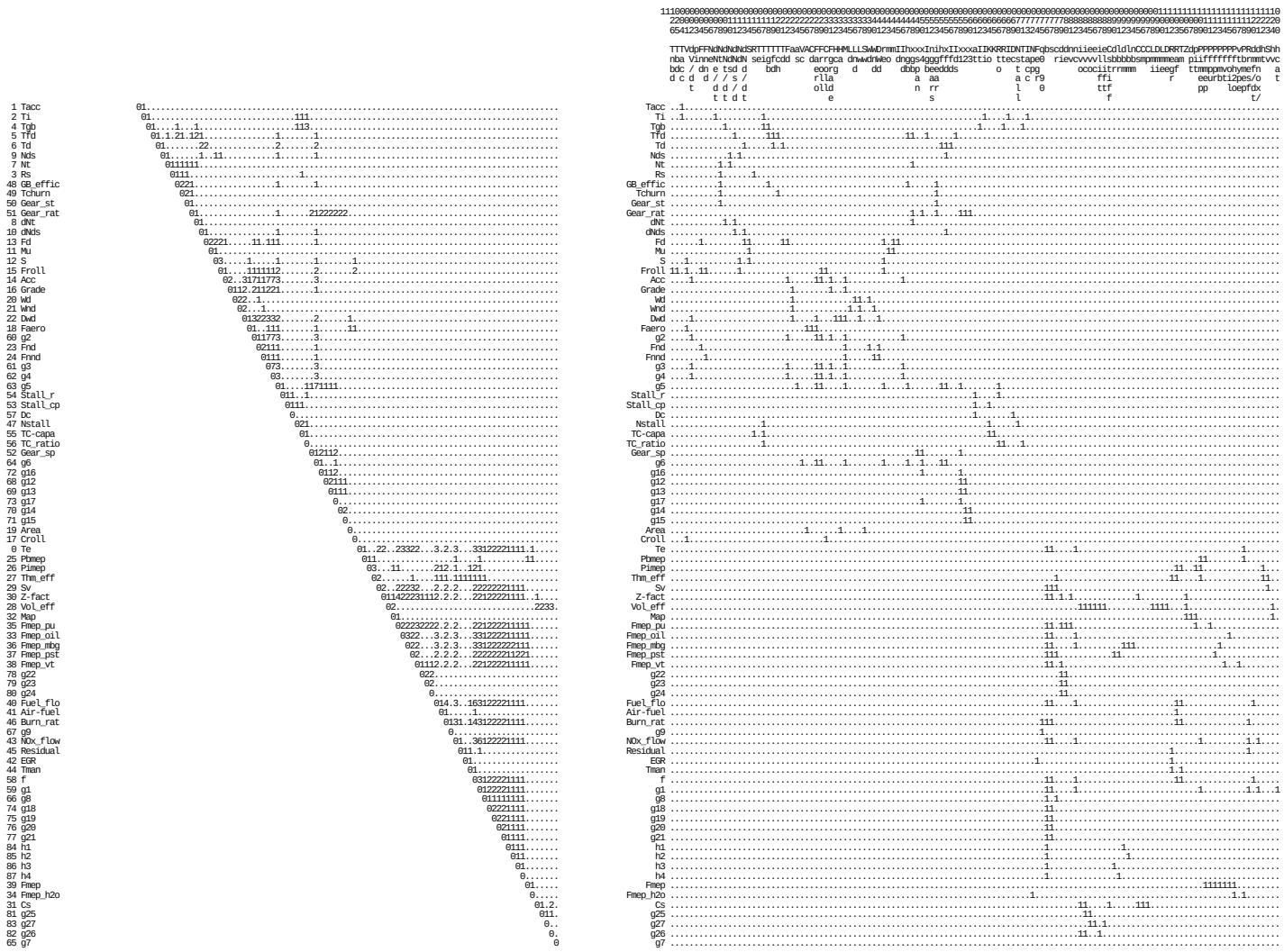

Figure 10. Partitioned graph and resulting FDT; $\mathbf{y} = (T_e, N_e, p_i)$ is temporarily removed from FDT.

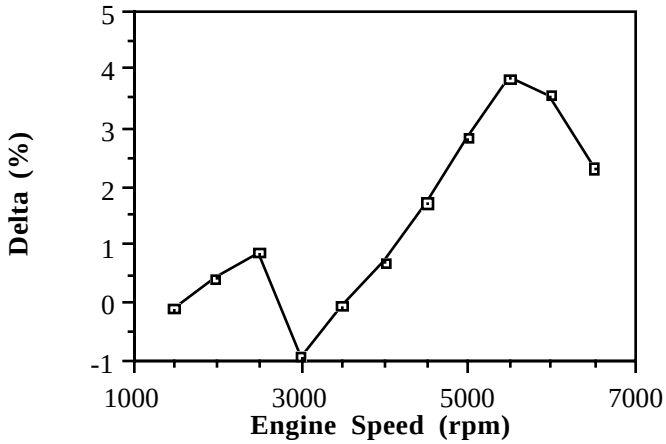

Figure 11. Relative improvement in volumetric efficiency from SP

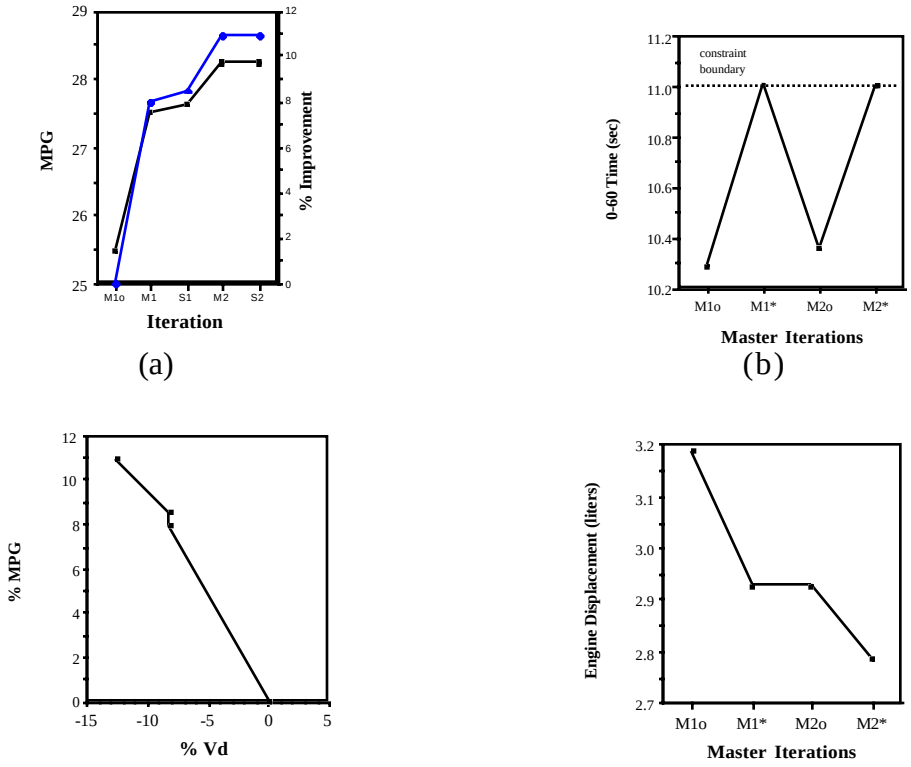

Figure 12. Iteration history of Master Problem variables.

Table I Summary of Coordination Strategy Iterations.

I	II	III	IV	V	VI	VII	VIII	IX	X	XI
			MP		SP		MP		SP	
			Initial	**Final**			**Intial**	**Final**		
MP	ξ		2.75	2.3179			2.3179	2.3493		
	ξ		1.55	1.4230			1.4230	1.4326		
	ξ		.72	0.5938			0.5938	0.6011		
	ξ		3.4666	3.4615			3.4615	3.4530		
	α		1.0	1.2000			1.2000	1.2000		
	Vd	liters	3.1856	2.9274			2.9274	2.7871		
					Inital	**Final**			**Initial**	**Final**
SP	b	mm	90.93		88.41	86.56			85.15	85.15
	s	mm	81.74		79.47	82.86			81.51	81.51
	c_r		9.25		9.25	9.30			9.37	9.37
	d_i	mm	43.2		42.0	41.11			40.45	40.45
	d_e	mm	36.73		35.8	34.97			34.4	34.4
	F_{egr}		1.0		1.0	1.37			1.37	1.37
	d_{br}	mm	54.56		53.05	51.94			51.09	51.09
	l_{br}	mm	19.62		19.10	18.70			18.39	18.39
	d_{bm}	mm	63.65		61.89	60.59			59.61	59.61
	l_{bm}	mm	22.2		21.66	21.21			20.86	20.86
	i_{vo}	deg	340.		340.	340.			340.	340.
	i_{vc}	deg	612.		612.	612.			612.	612.
	e_{vo}	deg	110.		110.	110.			110.	110.
	e_{vc}	deg	390.		390.	390.			390.	390.
	i_{lift}	mm	10.6		10.6	10.6			10.6	10.6
	e_{lift}	mm	10.6		10.6	10.6			10.6	10.6
	L_i	cm	31.		31.	41.4			38.31	38.31
	D_{i1}	cm	4.7		4.7	5.97			5.75	5.75
	D_{i2}	cm	3.45		3.45	3.81			3.68	3.68
	MPG_{m-h}	mi/g	25.46	27.49			27.62	28.23		
	NOx_{epa}	gm/	0.207	.2029			0.171	0.173		
	τ	sec	10.288	11.006			10.362	10.99		
	τ	sec	1.69	1.619			1.616	1.697		
	$S_{0\text{-}4}$	ft	92.58	92.94			93.28	90.05		
	α	%	47.2	47.2			47.2	47.2		
	V_c	mph	79.8	79.3			79.8	75.5		
	K_o	rpm/	238.3	324.5			324.5	324.5		
	R_o		2.90	3.48			3.48	3.48		
	N_{stall}	rpm	2074	2721			2728	2655		
	Te(Nstall	ft-lb	166.4		153.1	155.9			147.1	147.1
	N_{pp}	rpm	5150		5500	5250			5300	5300
	Power/l	hp/li	47.44		49.31	49.31			50.17	50.17
	Power	hp	151.1		144.3	144.3			139.7	139.7

APPENDIX A: Powertrain Model Summary

Table A.1: Summary of geometric, behavior, and state variables.

Index	Variable	Partition	Description
0	η_{cat}	1	Catalyst efficency
1	V	2	Vehicle velocity
2	dV/dt	2	Vehicle acceleration
3	p_i	y	Intake manifold pressure
4	F_{nd}	2	Normal force at driving wheels
5	F_{nnd}	2	Normal force at non-driving wheels
6	N_e	y	Engine speed
7	dN_e/dt	2	Engine acceleration
8	N_t	2	Torque converter turbine speed
9	dN_t/dt	2	Torque converter turbine acceleration
10	N_{ds}	2	Drive shaft speed
11	dN_{ds}/dt	2	Drive shaft acceleration
12	N_d	2	Driving axle speed
13	dN_d/dt	2	Driving axle acceleration
14	S	2	Slip ratio
15	R_s	2	Speed ratio across torque converter
16	T_e	y	Engine torque
17	T_i	2	Torque converter impeller torque
18	T_{gb}	2	Torque entering gearbox
19	T_{fd}	2	Torque entering final drive
20	T_{ch}	2	Churning losses in gear box
21	T_d	2	Torque at driving axle
22	F_d	2	Force at drving wheel/road interface
23	α	2	Grade angle
24	α_s	2	Starting grade angle
25	V_c	2	Cruising speed at 7% grade.
26	A	2	Vehicle frontal area
27	C_d	2	Vehicle body drag coefficient
28	F_{aero}	2	Aerodynamic resistance force
29	F_{roll}	2	Rolling resistance force
30	C_{roll}	2	Coefficient of rolling resistance
31	F_{grade}	2	Grade resistance force
32	H_{cg}	2	Height of center of gravity
33	H_a	2	Height of aerodynamic effort
34	M	2	Mass of vehicle
35	L_d	2	Distance from center of gravity to driving axle

Index	Variable	Partition	Description
36	L_{nd}	2	Distance from center of gravity to non-driving axle
37	L_w	2	Wheelbase
38	S_w	2	Length of axle
39	W_d	2	Weight distribution factor at driving wheel
40	W_{nd}	2	Weight distribution factor at non-driving wheel
41	ΔW_d	2	Dynamic axle weight
42	r_e	2	Effective tire radius
43	μ_o	2	Coefficient of adhesion
44	μ	2	Traction ratio
45	I_d	2	Rotational inertia of driving wheel
46	I_{nd}	2	Rotational inertia of non-driving wheel
47	η_{gb}	2	Power conversion efficiency of gearbox
48	ξ_{gb}	2	Speed reduction ratio of gearbox
49	ξ_{span}	2	Span ratio of gearbox
50	ξ_4	2	Fourth gear
51	I_{gb}	2	Rotational inertia of gear box
52	n_{gears}	2	Number of gears in gearbox
53	i_{gear}	2	Index of gear
54	η_{fd}	2	Power conversion efficiency at differential
55	ξ_{fd}	2	Reduction ratio at differential
56	I_{fd}	2	Rotational inertia of differential
57	I_{ds}	2	Rotational inertia of drive shaft
58	ξ_1	2	First gear
59	ξ_2	2	Second gear
60	ξ_3	2	Third gear
61	α_t	2	Torque converter impeller angle
62	I_t	2	Rotational inertia of torque converter turbine
63	I_i	2	Rotational inertia of torque converter impeller
64	K_o	2	Capacity factor of torque converter at stall speed
65	K	2	Capacity factor of torque converter
66	R_{to}	2	Torque ratio of torque converter at stall
67	R_t	2	Torque ratio of torque converter
68	I_e	2	Rotational inertia of engine
69	Dc	2	Diameter of torque converter
70	N_{stall}	2	Torque converter stall speed
71	T_t	2	Turbine torque
72	N_{pp}	1	Engine speed at peak power
73	I_{acc}	2	Inertia of accessories
74	F_{egr}	1	Egr factor
75	$\theta_{0\text{-}90}$	1	Burn duration
76	b	1	Bore
77	s	1	Stroke

Index	Variable	Partition	Description
78	c_r	1	Compression ratio
79	d_i	1	Intake valve diameter
80	d_e	1	Exhaust valve diameter
81	n_v	1	Number of valves
82	n_c	1	Number of cylinders
83	i_{vo}	1	Intake valve opening timing
84	i_{vc}	1	Intake valve closing timing
85	e_{vo}	1	Exhaust valve opening timing
86	e_{vc}	1	Exhaust valve closing timing
87	i_{lift}	1	Intake valve maximum lift
88	e_{lift}	1	Exhaust valve maximum lift
89	C_{stiff}	1	Valvetrain stiffness factor
90	d_{br}	1	Diameter of rod bearing diameter
91	l_{br}	1	Width of rod bearing
92	d_{bm}	1	Diameter of main bearing
93	l_{bm}	1	Width of main bearing
94	n_{bm}	1	Number of main bearings
95	C_s	1	Induction system discharge coefficient
96	C_m	1	Manifold discharge coefficient
97	C_p	1	Port discharge coefficient
98	L_{mi}	1	Intake manifold runner length
99	D_{mi}	1	Intake manifold runner diamter
100	L_{me}	1	Exhaust manifold runner length
101	D_{me}	1	Exhaust manifold runner diameter
102	R_{egr}	1	Exhaust gas recirculation
103	R_{af}	1	Air-fuel ratio
104	T_{acc}	2	Accessory torque
105	T_m	1	Temperature of charge in intake manifold
106	Z	1	Mach index
107	dp_t	1	Tuning pressure
108	p_{it}	1	Tuning manifold pressure
109	P_{imep}	1	Indicated mean effective pressure
110	P_{fmep}	1	Total friction mean effective pressure
111	P_{fpu}	1	Pumping mean effective pressure
112	P_{fpr}	1	Piston-ring interface friction mean effective pressure
113	P_{fmb}	1	Main bearing frcition mean effective pressure
114	P_{fvt}	1	Valvetrain friction mean effective pressure
115	P_{foil}	1	Oil pump friction mean effective pressure
116	P_{fh2o}	1	Water pump friction mean effective pressure
117	v_{type}	1	Valve train type
118	P_{bmep}	1	Brake mean effective pressure
119	R_{resf}	1	Total residual fraction in engine

Index	Variable	Partition	Description
120	dm_f/dt	1	Fuel flow rate
121	dm_{nox}/dt	1	NOx flow rate
122	η_t	1	Thermal efficiency
123	S_v	1	Surface-to-volume ratio
124	η_v	1	Volumetric efficiency
125	T_{bd}	2	Brake drag @ driving wheels
126	T_{bnd}	2	Brake drag @ non-driving wheels

Table A.2: Summary of Vehicle Optimization Model Equations.

f-index	Name	Equation	Index list
0	Te	T_e - 7.955 x 10 $^{-6}$ P_{bmep} b^2 s π /4 n_c	16, 118, 76, 77, 82
1	Tacc	T_{acc} - f (N_e).	104, 6
2	Ti	T_i - (T_e - T_{acc} - π/30(I_e + I_{acc} + I_i) dN_e/dt)	17, 16, 104, 68, 73, 63, 7
3	Rs	R_s - N_t/ N_e	15., 6, 8
4	Tgb	T_{gb} - (T_t - π/30 I_t dN_t/dt)	18, 62, 9,71
5	Tfd	T_{fd} - (T_{gb} η_{gb} ξ_{gb} - T_{ch} - π /30 (I_{gb} + I_{ds}) dN_{ds}/dt)	19, 18, 47, 48, 20, 51, 57, 11
6	Td	T_d - (T_{fd} η_{fd} ξ_{fd} - π/ 30 I_{fd} dN_{dr}/dt)	21, 19, 54, 55, 56, 13
7	Nt	N_t - ξ_{gb} N_{ds}	8, 48, 10
8	dNt	dN_t/dt - $\xi_{gb} dN_{ds}/dt$	9, 48, 11
9	Nds	N_{ds} -ξ_{fd} N_d	10, 55, 12
10	dNds	dN_{ds}/dt - ξ_{fd} dN_d/dt	11, 55, 13
11	Mu	μ – (1.07 μ_o (1 - e $^{-17.31\ S/(S-1)}$) - 0.285S/(S-1))	44, 43, 14
12	S	S - (1 - π/30 re N_d / V)	14, 42, 12, 1
13	Fd	F_d - (F_{nd} μ(S) + (1 - |sign (S)|) (T_d - π /30 I_d dN_d/dt) / r_e)	22, 4, 44, 14, 21, 45, 13, 42
14	Acc	(M + C I_{nd}) dV/dt - (F_d - F_{roll} - F_{grade} - F_{aero})	34, 2, 22, 29, 31, 28, 46
15	Froll	F_{roll} - (C_{roll} F_{nnd} + C_{roll} F_{nd} + (T_{bd} (N_d) + T_{bnd} (V/r_e))/r_e)	29, 30, 4, 5, 125, 126, 12, 1, 42
16	Grade	F_{grade} - (M g sin α,)	31, 34, 23,
17	Croll	C_{roll} - (0.05 (1. + V/100).	30 1
18	Faero	F_{aero} - (0.5 C_d A ρ_{air} V^2)	28, 27, 26, 1
19	Area	A - (0.9 Ha Sw)	26, 33, 38
20	Wd	W_d - (L_{nd} cos α / L_w)	39, 36, 23, 37
21	Wnd	W_{nd} - (L_d cos α / L_w)	40, 35, 23, 37
22	Dwd	ΔW_d - ((M dV/dt H_{cg} + Mg sin α H_{cg} + F_{aero} H_a) / L_w)	41, 34, 2, 32, 23, 28, 33, 37

23	Fnd	F_{nd} $-(W_d M g - \Delta W_d)$ (front wheel drive) $-(W_d M g + \Delta W_d)$ (rear wheel drive)	4, 39, 34, 41
24	Fnnd	F_{nnd} $-(W_{nd} M g + \Delta W_d)$ (front wheel drive) $-(W_{nd} M g - \Delta W_d)$ (rear wheel drive)	5, 40, 34, 41
25	Pbmep	$P_{bmep} - (P_{imep} - P_{fmep})$	118, 109, 110
26	Pimep	$P_{imep} - 3.479 \times 10^{-2} (pi_t / T_m) Q/R_{af)} \eta t.$	109, 108, 105, 103, 122
27	Thm_eff	$\eta_t - 0.9 (1 - c_r (-0.33 - .01 Regr/30)) f_C(\phi) + S_v (N_e/1500)^{0.5} (4.137/P_{imep})^{0.2}$	122, 78, 102, 103, 123, 6, 109
28	Vol_eff	$\eta_v - f(i_{vo}, i_{ve}, e_{vo}, e_{vc}, i_{lift}, e_{lift}, n_v, L_{mi}, D_{mi}, L_{me}, D_{me}, Z)$	124, 83, 84, 85, 86, 87, 88, 106, 98, 99, 100, 101
29	Sv	$S_v - (0.83 (12 s + (c_r - 1)(6 b + 4 s)) / (b s (2 + c_r))$	123, 78, 76, 77
30	Z-fact	$Z - (2 s Ne / (60 a_o Cs nv) (b/di)^2)$	106, 77, 6, 81, 95, 76, 79
31	Cs	$C_s - (C_{stiff} C_m C_p (i_{vc} - i_{vo})/180 (C_m^2 + C_p^2 - C_m^2 C_p^2)^{-0.5})$	95, 89, 96, 97, 84, 83
32	Map	$pi_t - (p_i + \Delta p_t (Z, \eta_v) (p_i - 33.86)/(67.68))$	108, 3, 107, 106, 124
33	Fmep_oil	$P_{foil} - ((4.6 - b^2 s \pi /4 n_c \times 10^{-6})/ 2.7 (Oil_{ld} - Oil_{hd}) + Oil_{hd})$	115, 76, 77, 82, 6
34	Fmep_h2o	$P_{fh2o} - (H2O_{lpd} + (H2O_{hpd} - H2O_{lpd})(P_{bmep}(N_{pp}) N_{pp}/895.2-54)/16)$	116, 118, 72, 6
35	Fmep_pump	$P_{fpu} - (p_a - p_{it} + 4.12 \times 10^{-9} (p_{it}/pa)^2 ((N_e s b^2 / (30 n_v))^2 (d_i^{-4} + d_e^{-4})$ $+ 0.178 \times 10^{-6} (p_{it}/ p_a)^2 (N_e s / 30)^2)$	111, 108, 6, 76, 77, 81, 79, 80,
36	Fmep_mainbrg	$P_{fmb} - (1.22 \times 10^5 d_{bm}/(b^2 s n_c) + 3.03 \times 10^{-4} Ne d_{bm}^3 l_{bm} n_b/(b^2 s n_c)$ $+ 1.35 \times 10^{-10} d_{bm}^2 N_e^2 n_b/ n_c)$	113, 92, 6, 76, 77, 82, 93, 94
37	Fmep_pist	$P_{fpr} - (3.03 \times 10^{-4} N_e d_{br}^3 l_{br} n_{br}/(b^2 s n_c) + 2.94 \times 10^{-1} N_e s / (30 b)$ $+ 4.06 \times 10^4 (1 + 1000/ N_e) b^{-2}$ $+ 6.89 p_i/p_a (0.088 c_r + 0.182 c_r (1.33 - 0.0238 Ne s /30000))$	112, 6, 90, 91, 76, 77, 3, 78, 94
38	Fmep_vtrain	$P_{fvt} - (10 F_{spvt}(vt_{type}, N_e) d_i^2 / (b^2 s \pi /4))$	114, 117, 6, 79, 76, 77
39	Fmep	$P_{fmep} - (P_{fpu} + P_{fpr} + P_{fmb} + P_{fvt} + P_{foil} + P_{fh2o})$	110, 111, 112, 113, 114, 115, 116
40	Fuel_flow	$\dot{m}_f - (3.479 \times 10^{-6} pi/T_m N_e n_c b^2 s \pi /(480 R_{af}))$	120, 3, 105, 6, 82, 76, 77, 103
41	Air-fuel	$R_{af} - f(p_i, N_e)$	103, 3, 6

42	EGR	R_{egr} - f (p_i, N_e, F_{egr})	102, 3, 6, 74
43	NOx_flow	$\dot{m}_{nox}$ - C_{nox} 50 e $^{(-R_{resf} * 12.88)}$ 7.955 x 10 $^{-6}$ $P_{imep} b^2 s \pi /4 n_c N_e /7122$	121, 119, 6, 76, 77, 82, 109
44	Tmanifold	T_m - (310 + R_{egr} 400) / (1 + R_{egr}/100)	105, 102
45	Residual	R_{resf} - f (R_{egr}, p_i)	119, 102, 3
46	Burn_rate	θ_{0-90} - F(N_e, b, s, R_{resf},R_{af}, p_i, T_m)	3, 6, 75, 76, 77, 103, 105., 119
47	Nstall	N_{stall} - K_o T_i $^{-0.5}$.	70, 64, 17
48	GB_effic	η_{gb} - f (T_{gb}, N_t, i_{gear})	47, 18, 8, 53
49	Tchurning	Tch - f (Nt, i_gear)	20, 8, 53
50	Gear_state	i_{gear} - f(p_i, N_t)	53, 3, 8
51	Gear_ratio	ξ_{gb} - f (i_{gear}, ξ_1, ξ_2, ξ_3, ξ_4)	48, 53, 58, 59, 60, 50
52	Gear_span	ξ_{span}- ξ_1/ξ_4	49, 50, 58
53	Stall_capac	K_o - K_{obase} α_t $^{1.7}$	64, 61
54	Stall_ratio	R_{to} - R_{obase} α_t	66, 61
55	TC-capac	K(R_s, K_o) - $N_e T_i^{-0.5}$	65,15 ,64 ,6 ,17
56	TC_ratio	R_t (R_s, R_{to}) - T_t/T_i	67, 66, 15, 71,17
57	Dc	$D_c = D_{cbase}$ α_t $^{-0.68}$	69, 61
58	f	$\dot{m}_f$	120, 3,105,6,82,76,77,103
59	g1	$\dot{m}_{nox}$ ηcat	0,121, 119, 16, 6,
60	g2	f (dV/dt,)	34,2,22,29,31,28,46
61	g3	f(dV/dt)	34,22,22,29,31,28,46
62	g4	f(dV/dt)	34,22,22,29,31,28,46
63	g5	sin α_s-(T_e(60 ξ_{fd} $\xi_1 V_s$/(2 r_e π)) ξ_{fd} ξ_1 $\eta_{fd}\eta_{gb}$ R_{to} - r_e (F_{roll} + F_{aero})) (r_e M g)$^{-1}$	24, 16, 55, 58, 42, 54, 47, 66, 29, 28, 34
64	g6	sin α_c - (T_e(60ξ_{fd} ξ_4 V_c/(2 r_e π)) ξ_{fd} ξ_4 $\eta_{fd}\eta_{gb}$ - r_e (F_{roll} + F_{aero})) (r_e M g)$^{-1}$	25, 16, 55, 50, 42,, 54, 47, 29, 28, 34
65	g7	$T_e(N_e)/T_{elug}(N_e)$ -1	16, 6

66	g8	c_r - 13.2 + 0.045 b	78, 76
	g9	$\theta_{0–90} - 70$	75
67	g12	1.6 - ξ_1 / ξ_2	58, 59
68	g13	ξ_1 / ξ_2 - 2.	58, 59
69	g14	1.2 - ξ_2 / ξ_3	59, 60
70	g15	ξ_2 / ξ_3 - 1.6	59, 60
71	g16	3.5- ξ_1 / ξ_4	58, 50
72	g17	ξ_1 / ξ_4 - 4.5	58, 50
73	g18	0.8 - b/s	76, 77
74	g19	b/s - 1.2	76, 77
75	g20	400 - π $b^2 s/ (4 n_c) \times 10^{-3}$	76, 77, 82
76	g21	π $b^2 s/ (4 n_c) \times 10^{-3}$ - 600	76, 77, 82
77	g22	$d_i + d_e$ -.88 b	79, 80
78	g23	0.85 - d_e/d_i	79,.80
79	g24	d_e/d_i - 0.87	79, 80
80	g25	i_{vo}-e_{vc} - 40	84, 85
81	g26	acc_{iv} (i_{vo} i_{vc} i_{lift}) - K_{acci}	83, 84, 87
82	g27	acc_{ev} (e_{vo} e_{vc} e_{lift}) - K_{acce}	85, 86, 88
83	h1	d_{bm} /b - K_{dm}	92, 76
84	h2	l_{bm} / b - K_{lm}	93, 76
85	h3	d_{br} / b - K_{dr}	90, 76
86	h4	l_{br} / b - K_{lr}	91, 76

TableA-3.
Bearing size parameters.

	In-line	V-engine	
		1 rod/pin	2 rods/pin
K_{dm}	.6	.7	.62
K_{lm}	.37	.35	.4
K_{dr}	.57	.6	.57
K_{lr}	.41	.36	.39

Appendix B: Parameters in Optimization Model

Table B.1: Summary of optimization model parameters.

Variable	Description	Value	Units
τ_0	Baseline 0-60 mph time	11	sec
τ_1	Baseline 5-20 mph time	1.81	sec
S_{o-4}	Distance traveled 4 seconds on max. accel	88.4	ft
α_s	Grade limit	30	%
V_c	Cruising speed @ grade	65	mph
A	Vehicle frontal area	22.7	ft^2
C_d	Vehicle body drag coefficient	.33	
H_{cg}	Height of center of gravity	20.5	in
M g	Weight of vehicle	3537	lbf
L_d	Distance from center of gravity to driving axle	40.28	in
L_{nd}	Distance from center of gravity to non-driving axle	65.72	in
L_w	Wheelbase	106	in
S_w	Length of axle	60.2	in
r_e	Effective tire radius	12.24	in
μ_o	Coefficient of adhesion	1.00	
I_d	Rotational inertia of driving wheel	.62	$lbf\text{-}ft\text{-}sec^2$
I_{nd}	Rotational inertia of non-driving wheel	.62	$lbf\text{-}ft\text{-}sec^2$
n_{gears}	Number of gears in gearbox	4	
I_{fd}	Rotational inertia of differential	.0124	$lbf\text{-}ft\text{-}sec^2$
I_t	Rotational inertia of torque converter turbine	.0874	$lbf\text{-}ft\text{-}sec^2$
I_i	Rotational inertia of torque converter impeller	.0293	$lbf\text{-}ft\text{-}sec^2$
I_e	Rotational inertia of engine	.164	$lbf\text{-}ft\text{-}sec^2$
N_{idle}	Engine idle speed	700	rpm
v_{type}	Valvetrain type	pushrod	
e_{type}	Engine type	V	
C_{stiff}	Valvetrain stiffness factor	.970	
C_s	System discharge coefficient	.325	
C_m	Manifold discharge coefficient	.650	
C_p	Port discharge coefficient	.413	
n_{bm}	Number of main bearings	4	
η_{cat}	Catalyst NOx effiecincy	0.90	

Table B.2: Brake drag torque.

Wheel rpm	Driving wheel (ft-lb)	Non-driving wheel (ft-lb)
0	1.598	1.137
280	2.368	1.467
420	2.753	1.632
560	3.063	1.768
700	3.337	1.884
841	3.611	2.000
2000	3.611	2.000

Table B.3: Gearbox efficiencies, inertias, lug limits, and churning losses.

		Gear 1	**Gear 2**	**Gear 3**	**Gear 4**
η		0.95	0.955	0.975	0.965
Igb	ft-lb/sec2	0.026	0.0622	0.04	0.045
Lug limit	rpm	open	700	1000	1250
	Tch @ rpm	ft-lb	ft-lb	ft-lb	ft-lb
	0	0.854	1.17	2.398	2.354
	500	0.854	1.17	2.398	2.354
	1000	0.979	1.679	3.004	3.292
	2000	1.058	1.971	3.508	4.096
	3000	1.471	2.283	3.996	4.896
	4000	1.775	2.6	4.813	6.213
	5000	2.267	3.279	5.704	7.992
	7000	4.4	6.4		
	8000	5.8	8.4		
	9000	7.3			

Table B.4: Base torque converter characteristics.

Impeller Driving			Turbine Driving		
R_S	T_r	K rpm/(ft-lb)$^{-1/2}$	R_S	T_r	K rpm/(ft-lb)$^{-1/2}$
0	2.900	238.3	1.001	1.1	50400
0.098	2.678	238.8	1.055	1.1	688.8
0.196	2.455	240.5	1.070	1.1	644.7
0.289	2.244	243.8	1.111	1.1	573.7
0.379	2.040	247.7	1.176	1.1	506
0.465	1.845	253.9	1.294	1.1	445.8
0.500	1.765	256.8	1.544	1.1	398.6
0.543	1.667	260.5	2.094	1.1	360.6
0.612	1.511	268.3	3.816	1.1	328.6
0.676	1.365	278.2			
0.730	1.243	289.4			
0.777	1.136	303.0			
0.815	1.050	318.1			
0.834	1.007	325.3			
0.848	1.000	333.1			
0.889	0.990	370.5			
0.917	0.990	409.7			
0.935	0.990	452.7			
0.946	0.990	496.8			
0.955	0.990	603.2			
0.958	0.990	671.9			
0.965	0.990	770.3			
0.974	0.990	934.8			
0.987	0.990	1304.5			
0.995	0.990	1830.4			
0.996	0.990	7200			
0.997	0.990	50400			

Table B.5: Specific valvetrain friction.

Engine Speed	Specific friction -kPa
499	7.653
1000	6.343
1500	5.585
2500	4.964
3000	4.413
3500	3.861
4500	3.172
5500	2.758
6500	2.344

Table B.6: Oil pump losses

RPM	Poil_ld (kPa)	RPM	Poil_hd (kPa)
500	3.09	500	2.01
1000	5.95	700	2.48
1500	8.38	2000	4.96
2000	10.28	4000	6.96
3000	13.39	6000	9.45
4000	16.07	6500	10.13
5000	16.75	7000	10.70
6000	17.86	10000	
6500	18.39		
7000	18.96		
10000			

Table B.7: Water pump losses.

RPM	Ph2o_hd (kPa)	RPM	Ph2o_ld (kPa)
385	0.36	413	0.85
769	0.72	826	1.03
1154	1.45	1240	1.32
1539	2.41	1653	2.06
1923	3.59	2066	3.23
2308	5.17	2479	4.61
2692	6.90	2893	6.18
3077	8.83	3306	7.90
3461	11.17	3719	10.17
3846	13.58	4132	12.51
4231	16.27	4546	14.63
4615	19.31	4959	16.76
5000	22.62	5500	19.68
5385	26.13	6000	22.26
5769	30.13	6500	24.85
6154	35.03	7000	27.58
6500	36.75		
7000	41.37		
10000			

Table B.8: Accessory losses.

Amps @ WOT - 26.0 Amps over m-h cycle - 16.5

Alternator Alt. RPM	Pulley ratio = 2.67 T @ 0 amp ft-lb	T @ 20 amp ft-lb	T @ 40 amp ft-lb	Acc. Torque Engine RPM ft-lb	Belt ft-lb	Front pump ft-lb
1000	0.09			500	0.08	1.83
1250	0.09	2.9		1000	0.08	1.833
1500	0.1	2.3	4.6	1500	0.08	2
1750	0.1	2	3.9	2000	0.08	2.17
2000	0.09	1.7	3.3	2500	0.08	2.33
2250	0.1	1.5	2.9	3000	0.08	2.42
2500	0.1	1.4	2.7	3500	0.08	2.58
2750	0.12	1.2	2.4	4000	0.08	2.75
3000	0.12	1.1	2.2	4500	0.08	2.92
3500	0.14	1	1.9	5000	0.08	2.83
4500	0.18	0.08	1.6	5500	0.08	3.08
5500	0.19	0.07	1.4	7000	0.08	5
6500	0.21	0.07	1.2	8000	0.08	6.5
8000	0.24	0.07	1.1	9000	0.08	8.3
				10000	0.08	10.2

Table B.9: Bearing size parameters.

	In-line	V-engine
		1 rod/pin	2 rods/pin
K_{dm}	.6	.7	.62
K_{lm}	.37	.35	.4
K_{dr}	.57	.6	.57
K_{lr}	.41	.36	.39

Table B.10: EGR schedule (in %).

RPM p_i ("Hg)	500	1000	1500	2000	2500	3000	3500	4000	4500	5000	5500	6000
6	0	0	0	0	0	0	0	0	0	0	0	0
8	0	0	0	0	0	0	0	0	0	0	0	0
10	0	0	0	0	0	0	7	7	0	0	0	0
12	0	0	0	6	0	8	9	0	0	0	0	0
14	0	0	0	8	8	10	10	8	0	0	0	0
16	0	0	0	10	10	12	11	4	0	0	0	0
18	0	0	0	9	12	15	11	2	0	0	0	0
20	0	0	0	0	7	10	0	0	0	0	0	0
22	0	0	0	5	11	17	5	0	0	0	0	0
24	0	0	0	0	7	10	0	0	0	0	0	0
26	0	0	0	0	4	3	0	0	0	0	0	0
28	0	0	0	0	0	0	0	0	0	0	0	0
29	0	0	0	0	0	0	0	0	0	0	0	0

Table B.11: Air-fuel ratio schedule.

RPM	500	1000	1500	2000	2500	3000	3500	4000	4500	5000	5500	6000
p_i ("Hg)												
6	14.6	14.6	14.6	14.6	14.6	14.6	14.6	14.6	14.6	14.6	14.6	14.6
8	14.6	14.6	14.6	14.6	14.6	14.6	14.6	14.6	14.6	14.6	14.6	14.6
10	14.6	14.6	14.6	14.6	14.6	14.6	14.6	14.6	14.6	14.6	14.6	14.6
12	14.6	14.6	14.6	14.6	14.6	14.6	14.6	14.6	14.6	14.6	14.6	14.6
14	14.6	14.6	14.6	14.6	14.6	14.6	14.6	14.6	14.6	14.6	14.6	14.6
16	14.6	14.6	14.6	14.6	14.6	14.6	14.6	14.6	14.6	14.6	14.6	14.6
18	14.6	14.6	14.6	14.6	14.6	14.6	14.6	14.6	14.6	14.6	14.6	14.6
20	14.6	14.6	14.6	14.6	14.6	14.6	14.6	14.6	14.6	14.6	14.6	14.6
22	14.6	14.6	14.6	14.6	14.6	14.6	14.6	14.6	14.6	13.0	13.0	13.0
24	13.5	13.8	13.8	14.6	14.6	14.6	14.6	14.6	13.0	13.0	13.0	13.0
26	13.0	13.0	13.0	13.0	14.6	14.6	13.0	13.0	13.0	13.0	13.0	13.0
28	13.0	13.0	13.0	13.0	13.0	13.0	13.0	13.0	13.0	13.0	13.0	13.0
29.4	12.4	12.4	12.4	12.4	12.4	12.5	12.4	12.5	12.6	13.0	13.0	13.0

Table B.12: Volumetric efficiency improvement in first iteration of subproblem.

Z- factor	η_v **Initial**	η_v **Final**
0.05290	0.7868	0.7868
0.07935	0.7606	0.7606
0.10578	0.7579	0.7579
0.13225	0.7643	0.7643
0.15869	0.7746	0.7740
0.18514	0.7842	0.7858
0.21159	0.7894	0.7925
0.23804	0.7909	0.7941
0.26449	0.7933	0.7999
0.29094	0.8024	0.8056
0.31739	0.8205	0.8128
0.34384	0.8308	0.8266
0.37029	0.8378	0.8373
0.39674	0.8456	0.8486
0.42318	0.8500	0.8557
0.44963	0.8487	0.8588
0.47608	0.8462	0.8606
0.50253	0.8445	0.8635
0.52898	0.8428	0.8664
0.55543	0.8318	0.8592
0.58188	0.8204	0.8517